Applied Energy 287 (2021) 116563

Contents lists available at ScienceDirect

Applied Energy

journal homepage: www.elsevier.com/locate/apenergy

Strategic design optimisation of multi-energy-storage-technology micro-grids considering a two-stage game-theoretic market for demand response aggregation

Soheil Mohseni [a,*], Alan C. Brent [a,b], Scott Kelly [c], Will N. Browne [a], Daniel Burmester [a]

[a] Sustainable Energy Systems, School of Engineering and Computer Science, Faculty of Engineering, Victoria University of Wellington, PO Box 600, Wellington 6140, New Zealand
[b] Department of Industrial Engineering and the Centre for Renewable and Sustainable Energy Studies, Stellenbosch University, Stellenbosch 7600, South Africa
[c] Institute for Sustainable Futures, University of Technology Sydney, Sydney, NSW 2007, Australia

HIGHLIGHTS

- A market-driven model is devised for long-term projections of incentive-aware loads.
- Responsive loads are integrated through dedicated aggregators for improved accuracy.
- A level playing field is provided for fuel cell electric vehicle-to-grid technology.
- An energy filter-based approach is employed to allocate various storage technologies.
- The model's potential in cutting a test micro-grid's lifetime costs by 21% is shown.

GRAPHICAL ABSTRACT

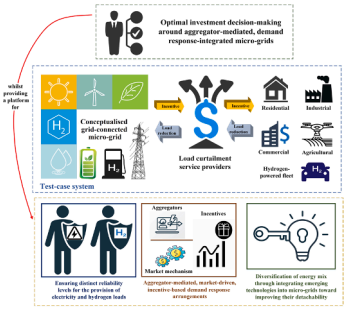

ARTICLE INFO

Keywords:
Sustainable energy systems
Demand-side management
Strategic energy planning
Optimal investment planning
Demand response aggregator
Game theory

ABSTRACT

While industrial demand response programmes have long been valued to support the power grid, recent advances in information and communications technology have enabled new opportunities to leverage the potential of responsive loads in less energy-dense end-use sectors. This brings to light the importance of accurately projecting flexible demand-side resources in the long-term investment planning process of micro-grids. This paper introduces a customer comfort-aware, demand response-integrated long-term micro-grid planning optimisation model. The model (1) draws on non-cooperative game theory and the Stackelberg leadership principles to understand and reflect the strategic behaviour of energy utilities, demand response aggregators, and end-consumers, (2) produces optimal trade-offs between power imported from the main grid and available demand response resources, (3) determines the cost-optimal resource allocation for energy infrastructure, including multiple energy storage systems, and (4) provides a level playing field for emerging technologies, such as power-to-gas and vehicle-to-grid interventions. The multi-energy-storage-technology test-case was effectively applied to achieve 100%-renewable energy generation for the town of Ohakune, New Zealand. Numerical simulation results suggest that the proposed incentive-compatible demand-side management market-clearing mechanism is able to estimate the cost-optimal solution for the provision of renewable energy during the planning phase. The cost-optimal system saves ~21% (equating to around US$5.5 m) compared to a business-as-usual approach, where

* Corresponding author.
E-mail address: soheil.mohseni@ecs.vuw.ac.nz (S. Mohseni).

https://doi.org/10.1016/j.apenergy.2021.116563
Received 13 August 2020; Received in revised form 20 January 2021; Accepted 23 January 2021
Available online 9 February 2021

the participation of end-users in demand response programmes is projected by running uniform price demand response auctions. The most salient distinction of the proposed two-stage (wholesale and retail) demand-side management market model is the continual process of trading, with incentive prices unique to each transaction.

Nomenclature

Indices and sets

$c \in C = \{PV, WT, MH, T, E, FC, HT, BP, B, SC, S, FCEV2G\}$ micro-grid components, the optimal size of which is under investigation: photovoltaic panels (*PV*), wind turbines (*WT*), micro-hydro turbines (*MH*), transformer (*T*), electrolyser (*E*), fuel cell (*FC*), hydrogen tank (*HT*), biopower plant (*BP*), battery bank (*B*), super-capacitor bank (*SC*), hydrogen station (*S*), and fuel cell electric vehicle-to-grid unit (*FCEV2G*)

$d \in D = \{1, 2, \cdots, 365\}$ day of the year-round micro-grid operation

$D^* = \{d_1^*, d_2^*, \cdots, d_K^*\}$ set of best-response load reductions contributed by all the customers

$D_{LA}^{j,*} = \{d^{k,j,*}, d^{-k,j,*}\}$ set of best-response strategies of all the customers signed up with the *j*-th aggregator

$es \in ES = \{B, SC, HT, FCEV\}$ energy storage media: battery bank (*B*), super-capacitor bank (*SC*), hydrogen tank (*HT*), and aggregated fuel cell electric vehicles' tanks (*FCEV*)

$I_{LA}^* = \{I_{LA}^{1,*}, I_{LA}^{2,*}, I_{LA}^{3,*}, I_{LA}^{4,*}, I_{LA}^{5,*}\}$ set of best-response incentive payments of aggregators

$j \in J$ responsive load aggregators

$k \in N_J$ customers enrolled with aggregator *j*

K set of all the micro-grid's customers

$p \in P_d \subset T$ day-specific peak consumption hour

$t \in T = \{1, 2, \cdots, 8760\}$ time-step of the year-round micro-grid operation

Parameters

$c_1^{k,j}$ discomfort tolerance coefficient of customer *k* of aggregator *j* [\$/kWh^2]

$c_2^{k,j}$ discomfort tolerance coefficient of customer *k* of aggregator *j* [\$/kWh]

C_{900}, C_{115}, C_{33} nameplate capacities of inverters [kW]

CV gross calorific value of biomass feedstock [kWh/kg]

δ_j load type-dependent demand response procurement factor; sectoral elasticity of customer-supplied demand response capacity

Δt time-step length [h]

$d_{cr}^{k,j}(t)$, $d_{ncr}^{k,j}(t)$ critical/non-critical portion of the load power demanded by the *k*-th customer subscribed to aggregator *j* at time-step *t* [kWh]

$d_{full}^{k,j}(t)$ full load power demanded by the *k*-th customer subscribed to aggregator *j* at time-step *t* [kWh]

$dis^{k,j,min}$, $dis^{k,j,max}$ lower/upper limit of the discomfort cost imposed on the *k*-th customer of aggregator *j* [\$]

DF derating factor of the PV module [%]

ξ_{CO_2} social cost of CO_2 emissions [\$/tCO_2]

η_{es} round-trip efficiency of storage medium *es* [%]

η_{FCEV2G} efficiency of the operation of the fuel cell electric vehicles in the vehicle-to-grid mode [%]

$\eta_{PV}, \eta_{MH}, \eta_{BP}, \eta_T, \eta_I, \eta_{SC}, \eta_B, \eta_E, \eta_{HT}, \eta_{FC}, \eta_S$ efficiency of the PV plant/micro-hydro plant/biopower plant/transformer/inverter/super-capacitor/battery/electrolyser/hydrogen tank/fuel cell/hydrogen station [%]

$\eta_{PV,DC/DC}, \eta_{MH,AC/DC}, \eta_{BP,AC/DC}$ PV plant's DC/DC converter efficiency, micro-hydro power plant's AC/DC converter efficiency, biopower plant's AC/DC converter efficiency [%]

E_{CO_2} CO_2 emission factor of the biopower plant [kg-CO_2/kg-feedstock]

$E_{es,min}$, $E_{es,max}$ lower/upper capacity limit of storage medium *es* [kWh]

$F(t)$ river streamflow rate at time-step *t* [m^3/s]

g acceleration of gravity [m/s^2]

h wind turbine hub height [m]

h_g micro-hydro turbine gross head [m]

h_{ref} reference height of wind speed records [m/s]

HHV_{H_2} higher heating value of hydrogen [kWh/kg]

i_{MGO} step size for the micro-grid operator-determined incentive [\$/kWh]

$I_G(t)$ global solar irradiance on the horizontal surface at time-step *t* [kW/m^2]

$I_{LA}^{j,min}$, $I_{LA}^{j,max}$ lower/upper limit of the incentives determined by aggregator *j* [\$/kWh]

I_{MGO}^{min}, I_{MGO}^{max} lower/upper limit of the micro-grid operator-offered incentives [\$/kWh]

I_{ref} reference solar irradiance [kW/m^2]

$Iter_{max}$ maximum number of iterations

K DC gain of the transfer function

K_p PV module's temperature coefficient [%/°C]

$LPSP_e^{max}$, $LPSP_{H_2}^{max}$ maximum allowable loss of power supply probability in supplying electricity/hydrogen [%]

$M_{BD}(t)$ biomass feedstock mass consumption rate at time-step *t* [kg/h]

N_{cust}^j number of customers enrolled with aggregator *j*

N_c^{max} upper limit of the size (capacity/quantity) of component *c*

N_{SA} number of search agents of the optimisation algorithm

$NMOT$ nominal PV module operating temperature [°C]

ρ water density [kg/m^3]

$P_{es}^{ch,max}$, $P_{es}^{dch,max}$ upper limit of the charging/discharging rate of storage medium *es* [kW]

$P_{es}^{ch,min}$, $P_{es}^{dch,min}$ lower limit of the charging/discharging rate of storage medium *es* [kW]

$P_{FCEV2G}^{max}(t)$ maximum V2G power at time-step *t* [kW]

$P_{FC,r}, P_{E,r}$ rated capacity of each fuel cell/electrolyser stack [kW]

$P_L(t)$ load power demand at time-step *t* [kW]

$P_{L,max}$ maximum electrical load on the micro-grid [kW]

$P_{MH,r}$, $P_{BP,r}$ rated capacity of each micro-hydro turbine/biopower plant [kW]

$P_{PV}(t)$, $P_{WT}(t)$, $P_{MH}(t)$, $P_{BP}(t)$ power output from the PV/wind turbine/micro-hydro/biopower plant at time-step *t* [kW]

$P_{PV,r}$ rated capacity of the PV module under standard test conditions [kW]

$P_S(t)$ hydrogen power demand of the station at time-step *t* [kW]

pen_{const} penalty term added to the life-cycle cost function where constraints are not met [\$]

π_{ex}, $\pi_{im}(t)$ per-unit income from electrical energy exports [\$/kWh], per-unit cost of electrical energy imports at time-step *t* [\$/kWh]

π_{FCEV2G} per-unit premium tariff rate for V2G power [\$/kWh]

Q quality factor of the low-pass energy filter

t_{up} minimum up-time of the electrolyser, fuel cell, and biopower plant [h]

$T_a(t)$ ambient temperature at time-step *t* [°C]

$T_m(t)$ PV module temperature at time-step *t* [°C]

T_{STC} PV module temperature under standard test conditions [°C]
V_h normalised wind speed profile to the wind turbine hub height [m/s]
V_{ref} reference wind speed profile [m/s]
ω_0 cut-off frequency [dB]
γ wind shear exponent

Variables

$cost_{em}(t)$ total penalties imposed for emissions at time-step t [$]
$cost_{FCEV2G}(t)$ cost associated with the FCEV2G operations at time-step t [$]
$cost_{im}(t)$ cost of electricity import at time-step t [$]
$d^{k,j}(t)$ load reduction contributed by the k-th customer of aggregator j at time-step t [kWh]
$d^{k,j,*}(t)$ best-response strategy taken by the k-th customer subscribed to the j-th aggregator for load reduction at time-step t [kWh]
$D_{def}(t)$ capacity deficit to meet the loads at time-step t [kWh]
$D^j_{LA}(t)$ load reduction contributed by aggregator j at time-step t [kWh]
$dis^{k,j}(t)$ discomfort cost imposed on the k-th customer subscribed to aggregator j at time-step t [$]
$E_{es}(t)$ energy content of storage medium es at time-step t [kWh]
$E_{SC}(t)$, $E_B(t)$, $E_{HT}(t)$ energy content of the super-capacitor/battery bank/hydrogen tank at time-step t [kWh]
$I^j_{LA}(t)$ incentive payment offered by aggregator j for load reduction at time-step t [$/kWh]
$I^{j,*}_{LA}(t)$ best-response incentive payment for load reduction offered by aggregator j at time-step t [$/kWh]
$I_{MGO}(t)$ rate of micro-grid operator-posted incentive payments for load reduction at time-step t [$/kWh]
$I^*_{MGO}(t)$ globally-optimum incentive payment for load reduction offered by the MG operator at time-step t [$/kWh]
$income_{ex}(t)$ income from electricity export at time-step t [$]
$LPSP_e$, $LPSP_{H_2}$ loss of power supply probability in supplying electricity/hydrogen [%]
$m_{HT}(t)$ mass of hydrogen stored in the tank at time-step t [kg]
N_B optimal capacity of the overall battery bank [kWh]
N_{FCEV2G} optimal capacity of the fuel cell electric vehicle-to-grid system [kW]
N_{HT} optimal capacity of the hydrogen tank [kg]
N_I optimal capacity of the electrical loads' overall power inversion system [kW]
N_{PV}, N_{WT}, N_{MH}, N_{BP}, N_E, N_{FC}, N_{SC} optimal quantity of PV modules/wind turbines/micro-hydro turbines/biopower units/electrolyser stacks/fuel cell stacks/super-capacitor modules
N_S optimal capacity of the hydrogen refuelling station [kg-H_2/h]
N_T optimal capacity of the transformer [kVA]
N_{900}, N_{115}, N_{33} optimal quantity of 900-kW/115-kW/33-kW inverters
N_{1600}, N_{400}, N_{100} optimal quantity of 1600-kWh/400-kWh/100-kWh battery packs
NPC_c net present cost of component c [$]
NPC_I net present cost of the inverter [$]
$OC_{MG}(t)$ operational cost of offsetting power deficit at time-step t [$]
$OC^*_{MG}(t)$ globally-optimum operational cost of the micro-grid to address the shortage of power generation capacity at time-step t [$]
$P_{ch}(t)$, $P_{dch}(t)$ total charging/discharging power of the hybrid battery/super-capacitor storage system at time-step t [kW]
$P_{ch,HF2}$, $P_{dch,HF2}$ charging/discharging power of the super-capacitor bank [kW]
$P_{ch,LF2}$, $P_{dch,LF2}$ charging/discharging power of the battery bank [kW]
$P_E(t)$ power consumed by the electrolyser at time-step t [kW]
$P_{E-HT}(t)$ hydrogen power directed from the electrolyser to the hydrogen tank at time-step t [kW]
$P^{ch}_{es}(t)$, $P^{dch}_{es}(t)$ charging/discharging rate of energy storage medium es at time-step t [kW]
$P_{FC}(t)$ power generated by the fuel cell at time-step t [kW]
$P_{FCEV2G}(t)$ aggregated vehicle-to-grid power provided by fuel cell electric vehicles at time-step t [kW]
$P_{HT-FC}(t)$ hydrogen power directed from the hydrogen tank to the fuel cell at time-step t [kW]
$P_{HT-S}(t)$ hydrogen power directed from the hydrogen tank to the station at time-step t [kW]
$P_{im}(t)$, $P_{ex}(t)$ imported/exported electricity at time-step t [kW]
$P_{SH}(t)$, $P_{EX}(t)$ shortage/excess of renewable power generation at time-step t [kW]
$P_{SH-LF1}(t)$, $P_{SH-HF1}(t)$ low-/high-frequency component of the renewable power shortage signal at the first low-pass filter output at time-step t [kW]
$P_{SH-LF2}(t)$, $P_{SH-HF2}(t)$ low-/high-frequency component of the renewable power shortage signal at the second low-pass filter output at time-step t [kW]
$P_{EX-LF1}(t)$, $P_{EX-HF1}(t)$ low-/high-frequency component of the renewable power excess signal at the first low-pass filter output at time-step t [kW]
$P_{EX-LF2}(t)$, $P_{EX-HF2}(t)$ low-/high-frequency component of the renewable power excess signal at the second low-pass filter output at time-step t [kW]
$Pr^j_{LA}(t)$ profit gained by aggregator j at time-step t [$]
$Q_L(t)$, $Q_{H_2}(t)$ unmet electrical/hydrogen load demand at time-step t [kW]
$U^{k,j}(t)$ utility of the customer k serviced by aggregator j at time-step t [$]

Functions

$H(s)$ low-pass energy filter transfer function
$\underset{20-yr}{NPV}(z)$ net present value of cost component z over the 20-year life of the project [$]
$\underset{20-yr}{NPC_c}$ net present cost of micro-grid component c over the 20-year life of the project [$]
$\underset{20-yr}{NPC_I}$ net present cost of the overall power inverter over the 20-year life of the project [$]
OC_{MG} hourly operational cost function of the micro-grid [$]
$\lfloor\cdot\rfloor$ floor function
$\lceil\cdot\rceil$ ceiling function

1. Introduction

One of the principal advantages of making the electricity grid "smart" is that it enables consumers to proactively engage in electricity markets and benefit from demand-side management (DSM) schemes designed and incentivised by utilities to curtail/interrupt or shift a proportion of electricity demand, and thereby flatten the load power profile–and improve the load factor. While demand response (DR) programmes have been in use to improve the energy efficiency of industrial consumers for years, the expansion of the concept to include less energy-

dense demand sectors, namely the residential, agricultural, and commercial sectors, as well as electrified transport, is enabled by recent advancements in information and communications technology (ICT), which have substantially contributed to the development of advanced metering infrastructure [1,2]. Recent studies have revealed that the consideration of DSM strategies in the optimum investment planning phase of renewable and sustainable energy systems (RSESs) for domestic applications can offer cost savings of about 15% to nearly 35% (depending on the participation rate of end-users in the DR programmes), whilst preserving consumer comfort standards [3,4,5]. That is, the proper integration of DR programmes into RSESs would result in a win–win–win situation–the third winner being the environment, as they will accelerate the transition to a low-carbon energy economy and a world run on green energy.

1.1. Long-term, demand response-integrated micro-grid infrastructure planning background

A reformed formulation of the micro-grid (MG) equipment capacity-planning problem is required to make effective use of the economic opportunities offered by DSM processes to support decision-making in developing cost-effective RSESs [6]. A solution to the optimal DR-integrated MG design problem identifies the least-cost combination of the size of the components of the system over a decades-long–often spanning 20–30 years–investment planning horizon to meet the projected demand for energy, while leveraging the potential of responsive loads [7,8].

Recent review studies have focused on discussing methods and trends for harvesting the potential of the demand-side flexibility to contribute significantly to energy affordability in energy networks with a high penetration of distributed renewables. Gelazanskas and Gamage [9], Haider et al. [10], Esther and Kumar [11], Wang et al. [12], Robert et al. [13], as well as, more recently, Jordehi [14] have scrutinised various approaches to implementing DR arrangements, while optimally designing RSESs, with a particular focus on residential DR resources. Moreover, various types of DSM strategies have been incorporated in the formulation of the MG capacity-optimisation models. This implies that DR programmes are well-analysed for the planning of RSESs, a statement that has likewise been made in the context of different DSM business models in electricity markets [15,16], as well as for the optimal operational scheduling (energy management) of RSESs [12].

There have also been attempts to exploit other types of DR structures for the optimal capacity planning of RSESs. For instance, Kahrobaee et al. [17] devised a particle swarm optimisation (PSO)-based planning model for a smart home nano-grid that utilises the real-time pricing (RTP) scheme, which allows for leveraging the historical records of the price elasticity of demand for personalised dynamic pricing. In another instance, Yu et al. [18] proposed a robust flexible-programming approach for the integration of renewables into a municipal energy system, which runs a critical peak pricing (CPP) rate structure. Moreover, Varasteh et al. [19] employ a hybrid direct load control-time-of-use (DLC-ToU) DR framework to drive down the whole-life cost of a grid-tied combined heat and power (CHP) MG.

In addition, some studies have explored the potential of vehicle-to-grid (V2G) technologies and electric vehicle (EV) charging/discharging coordination through DSM mechanisms in driving economic sustainability improvement for renewable energy development projects. For instance, Cardoso et al. [20] have proposed a DLC decision model for the aggregated energy scheduling of EVs and demonstrated its distinctive contribution to reducing the lifetime cost of a multiple energy carrier MG, while considering the uncertainty associated with the EV driving schedules. In another instance, Hosseinnia et al. [21] have provided further evidence of the utility and economic benefits of EV fleet trip level energy management and V2G connectivity in the context of sustainable energy system design and planning. Moghaddas-Tafreshi et al. [22] have also underlined the potential of optimal charging/discharging scheduling of plug-in hybrid EVs in improving the profitability of an energy hub and reaping cost-savings for vehicle owners, while addressing the uncertainty associated with the power consumption of vehicles during trips. Table 1 summarises the most rigorous studies carried out to date on the integration of demand-side resources (for the strategic planning of energy demand) in the long-term capacity optimisation models of RSESs (listed in ascending order of publication date), whilst additionally situating this study in the context of the existing literature.

1.2. Demand response-integrated life-cycle planning of micro-grids: knowledge gaps and proposition

As Table 1 indicates, there is a growing body of literature lending support to the integration of DSM frameworks into the design phase of RSESs. However, as far as can be ascertained, no single study has evaluated the attitude of neither end-users nor electricity providers in relation to adopting these practices during the optimal design and planning process of RSESs. Accordingly, oversimplified assumptions have commonly been made in the literature regarding the available capacity of responsive loads, which have substantially reduced the accuracy of projections. That is, many hypotheses regarding the degree of end-users' participation in the DR schemes are not well-grounded. To aid the associated asset-allocation decision-making procedure, a long-term, DR-integrated MG investment planning approach needs to model the involvement of aggregator-mediated customers in the DR programmes in a systematic, market-driven approach. The market-driven approach needs to capture the dynamic nature of strategic interactions between rational, utility-maximising active economic agents in an aggregator-mediated DSM market. More specifically, the approach needs to identify the reaction and commitment of different classes of customers mediated by third-party demand response aggregators (DRAs), when exposed to variations in the economic incentives for load curtailment/shifting. In this context, the DRAs round up parcels of interruptible loads to enable them to reach the sufficient scale required for selling services to the system operator(s) [43,44,45]. In addition, more work is needed to evaluate the effect of different levels of discomfort experienced by different customer classes on the economic feasibility of renewable energy projects as the characterisation of aggregator-mediated customer comfort constraints during the planning phases of RSESs is less well explored. To assist decision-makers in designing cost-optimal sustainable energy systems consistent with the expectations of their customers, it is critically important to devise accurate models aimed at reflecting user values and preferences (which furnish the basis for service flexibility) in the design of MG projects. This brings to light the need for an investment decision-making framework that accommodates end-users' preferences (which could be derived from their energy service needs and the relative values they place on them) within the long-term MG capital-investment plans.

1.3. Objective

The main objective of the paper is to demonstrate the potential of aggregator-mediated, incentive-based, market-driven DSM programmes tailored to small- to medium-scale end-consumers in improving the economic viability of community-scale MG systems. Accordingly, the paper expands the boundaries of knowledge and understanding of the positive impacts of altering energy consumption behaviour of different types of electrical loads–through effective incentive-based DR programmes–on the cost-optimal design of MGs. Also, a secondary objective of the paper is to ascertain the technological competence and cost-competitiveness of utilising hydrogen as an energy vector in community-scale MGs for niche applications–inter-seasonal energy storage to meet seasonal demand, and hydrogen mobility to decarbonise the transport sector.

More specifically, the paper contributes to the trend of the

Table 1
Summary of the studies on the provision of the DSM procurements in the long-term investment planning of the RSESs.

Reference	Test-case system configuration	DSM scheme	Flexible loads	V2G capabilities	DR-inherent uncertainties	Multi-temporal reserve procurement	Aggregator-mediated customer comfort characterisation	Modelling approach	Objective(s)	Solution algorithm	Case study area
Martins and Borges, 2011 [23]	A typical active distribution grid with a high share of renewables	ICSs	Unspecified	×	×	×	×	Stochastic	LCCM	GA	A typical distribution network in Brazil
Kahrobaee et al., 2013 [17]	A grid-connected WT/BESS nano-grid	RTP	SRAs	×	×	×	×	Stochastic	LCCM	PSO	A typical house in the U.S.
Cardoso et al., 2014 [20]	A grid-connected PV/ST/ICE/MT/GT/FC/BESS/AC MG	DLC	EV-charging	√	×	×	×	Stochastic	LCCM	DER-CAM tool	San Francisco, CA, U.S.
Zhu et al., 2015 [24]	An off-grid PV/WT/BESS/DG MG	DLC	HVAC	×	×	×	×	Deterministic	LCCM	NP	Shanghai, China
Atia and Yamada, 2016 [25]	A grid-tied PV/WT/BESS MG	DLC	SRAs and EV-charging	×	×	×	×	Stochastic	LCCM	MILP	Okinawa, Japan
Pazouki and Haghifam, 2016 [26]	A WT/MCHP/boiler/BESS/TESS energy hub	DLC	Unspecified	×	×	×	×	Stochastic	LCCM	MILP	Unspecified
Schachter et al., 2016 [27]	A typical smart distribution grid with deep renewable penetration	DLC	Unspecified	×	√	×	×	Stochastic	LCCM	SDM	Unspecified
Yu et al., 2017 [18]	A WT/PV/BP/coal/gas municipal energy system	CPP	Unspecified	×	×	×	×	Stochastic	LCCM	RFP	Qingdao, China
Chauhan and Saini, 2017 [28]	A stand-alone PV/WT/BESS/DG/BP/MHPP MG	DLC	Smart appliances of the residential, commercial, agricultural, and community sectors	×	×	×	×	Deterministic	LCCM	DHS	Chamoli, India
Nojavan et al., 2017 [29]	The standard IEEE 33-bus distribution network	ToU	Unspecified	×	×	×	×	Stochastic	LCCM and reliability maximisation	MINLP	Unspecified
Amrollahi and Bathaee, 2017 [30]	A grid-connected PV/WT/BESS	DLC	Unspecified	×	×	×	×	Deterministic	LCCM	MILP	An unnamed forestry camp, northwest of Iran
Chen et al., 2018 [31]	A grid-tied PV/WT/BESS MG	DLC	SRAs and HVAC	×	×	×	×	Stochastic	LCCM and reliability maximisation	MILP	Unspecified
Zheng et al., 2018 [32]	A grid-tied PV/BP/boiler MG	ToU	Unspecified	×	×	×	×	Stochastic	LCCM	LP	Davis, CA, U.S.
Xiao et al., 2018 [33]	A modified IEEE 33-bus distribution network with deep penetration of renewables	Hybrid DLC-ICSs	Unspecified thermal and electrical loads	×	×	×	×	Stochastic	LCCM	MBGO	Unspecified
Husein and Chung, 2018 [34]	An on-grid PV/WT/MHPP/GPP/BP MG	ToU	Unspecified	×	√	×	×	Stochastic	LCCM	ESM	Seoul, South Korea
Gazijahani and Salehi, 2018 [35]	A modified IEEE 33-bus distribution network with high penetration of renewables	CPP	Unspecified	√	×	×	×	Deterministic	LCCM	RMILP	Unspecified

(*continued on next page*)

Table 1 (*continued*)

Reference	Test-case system configuration	DSM scheme	Flexible loads	V2G capabilities	DR-inherent uncertainties	Multi-temporal reserve procurement	Aggregator-mediated customer comfort characterisation	Modelling approach	Objective(s)	Solution algorithm	Case study area
Amir et al., 2018 [36]	A grid-connected PV/BESS/boiler/TESS/MCHP MG	ToU	Unspecified	×	×	×	×	Deterministic	LCCM	GA	Unspecified
Mohseni et al., 2018 [37]	An off-grid PV/WT/battery MG	DLC	EV-charging	×	×	×	×	Deterministic	LCCM	GA	Kish Island, Iran
Nazari and Keypour, 2019 [38]	An on-grid PV/WT/BESS/MT MG	DLC	SRAs, PWS, and HVAC	×	×	×	×	Stochastic	LCCM	MILP	Unspecified
Prathapaneni and Detroja, 2019 [39]	A stand-alone PV/BESS/DG MG	DLC	EV-charging and PWS	×	×	×	×	Stochastic	LCCM	MINLP	Hyderabad, India
Hosseinnia et al., 2019 [21]	An on-grid PV/WT/BESS/boiler/MCHP/TESS MG	ToU	SRAs	√	×	×	×	Stochastic	LCCM and GHGEM	TSA	Unspecified
Bhamidi and Sivasubramani, 2019 [40]	A grid-connected PV/WT/BESS/MT/DG MG	ToU	SRAs and EV-charging	×	×	×	×	Deterministic	LCCM and GHGEM	NSGA-II	San Angelo, TX, U.S.
Varasteh et al., 2019 [19]	A multi-carrier PV/WT/CCHP/boiler/BESS MG	Hybrid DLC-ToU	SRAs	×	×	×	×	Deterministic	LCCM	MINLP	Unspecified
Mohseni et al., 2019 [41]	A grid-independent PV/WT/BESS MG	DLC	SRAs and EV-charging	×	×	×	×	Deterministic	LCCM	MFOA	Hengam Island, Iran
Amir and Azimian, 2020 [8]	A grid-connected PV/MCHP/BESS/TESS multiple energy carrier MG	Hybrid DLC-ToU	Unspecified	×	×	×	×	Stochastic	LCCM	GA-MINLP	Unspecified
Salyani et al., 2020 [42]	The standard IEEE 33-bus distribution network	RTP	EV-charging	√	√	×	×	Stochastic	LCCM and GHGEM	MINLP	Unspecified
This study	A grid-tied PV/WT/MHPP/BP/FC/BESS/SC MG	ICSs	SRAs and FCEVs	√	√	√	√	Deterministic	LCCM	MFOA	Ohakune, New Zealand

Key: AC = Absorption Chiller, BESS = Battery Energy Storage System, BP = Biopower Plant, CA = California state, CPP = Critical Peak Pricing, CCHP = Combined Cooling, Heating, and Power, DER-CAM = Distributed Energy Resources-Customer Adoption Model, DG = Diesel Generator, DHS = Discrete Harmony Search, DLC = Direct Load Control, ESM = Enumeration Search Method, EV = Electric Vehicle, FC = Fuel Cell, FCEV = Fuel Cell Electric Vehicle, GA = Genetic Algorithm, GHGEM = Greenhouse Gas Emissions Minimisation, GPP = Geothermal Power Plant, GT = Gas Turbine, HVAC = Heating, Ventilation, and Air Conditioning, ICE = Internal Combustion Engine, ICSs = Interruptible/Curtailable Services, LCCM = Life-Cycle Cost Minimisation, LP = Linear Programming, MBGO = Metamodel-Based Global Optimisation, MCHP = Micro-Combined Heat and Power, MG = Micro-Grid, MHPP = Micro-Hydro Power Plant, MILP = Mixed-Integer Linear Programming, MINLP = Mixed-Integer Nonlinear Programming, MFOA = Moth-Flame Optimisation Algorithm, MT = Micro-Turbine, NP = Nonlinear Programming, NSGA-II = Non-dominated Sorting Genetic Algorithm II, PSO = Particle Swarm Optimisation, PV = Photovoltaic, PWS = Pumped Water Storage, RFP = Robust Flexible Programming, RMILP = Robust MILP, RTP = Real-Time Pricing, SC = Super-Capacitor, SDM = Supply-Demand Matching, SRAs = Smart Residential Appliances, ST = Solar Thermal, TESS = Thermal Energy Storage System, ToU = Time-of-Use, TSA = Tabu Search Algorithm, TX = Texas state, WT = Wind Turbine.

conservation of energy through procuring DSM provisions for the strategic decision-making related to the optimal mix of distributed energy resources (DERs) to be integrated into RSESs–which is discussed in the literature review in Section 1.1. Accordingly, this study puts forward a novel long-term, comfort-preserving MG equipment capacity-planning decision-making framework that offers a new solution to fill the literature voids identified in Section 1.2. Notably, this paper makes the following key contributions:

- The strategic interactions between the MG operator (utility), monopoly DRAs, and end-consumers are characterised using an equitable market model for DR aggregation in community-scale renewable energy projects using tools borrowed from non-cooperative game theory [46] and the endogenous Stackelberg leader–follower relationships[1] [47]. The proposed DSM market model is designed on the basis of interruptible DR programmes and accounts for the elasticity of customer-supplied DR capacity (load type-dependent DR procurement factor).
- The proposed DSM market design is integrated into a standard model of long-term, *meta*-heuristic-based capacity planning of grid-connected MGs to elucidate the contributions of more accurate DR resource projections in improving the economic viability of MG development projects.
- A novel hydrogen-based MG system is conceptualised, which is the first to capture the potential of the fuel cell electric vehicles in vehicle-to-grid operation (FCEV2G) technology in improving the dispatchability of 100%-renewable MG systems and, in turn, ensuring the economic sustainability of strategic MG investment planning decisions.
- The application of the energy filter-based approach to scheduling energy storage infrastructure is expanded to multiple energy storage technologies, namely: hydrogen storage, vanadium redox flow batteries, and super-capacitors (SCs). This provides a platform to more efficiently address the intermittency of renewables by economically dispatching different backup systems running at various temporal resolutions, namely: seasonal, inter- and intra-day, and transient.

1.4. Structure of paper

The rest of this paper is organised as follows. Section 2 mathematically defines the conceptualised stand-alone, multi-energy-storage-technology MG architecture employed as a test-case to evaluate the utility and effectiveness of the proposed two-stage market-driven DSM business model. The proposed interruptible DR scheduling framework is presented in Section 3. Section 4 integrates the proposed DSM framework into a standard *meta*-heuristic-based MG capacity planning model. A case study analysis is carried out in Section 5. Finally, conclusions are made in Section 6.

A schematic outline of the paper, which illustrates the steps followed in this study and their interconnectedness, is set out in Fig. 1.

2. Test-case micro-grid system

The conceptualised grid-connected, DC-coupled, multiple energy carrier MG test-case system (see Fig. 2) is envisioned to supply green power and transportation fuel to communities residing in the vicinity of, or within relatively short distances from, the main power grids. Also, it serves five different categories of energy demand: (1) residential, (2) agricultural, (3) commercial, and (4) industrial load power demands, as well as (5) the demand for hydrogen (through dedicated hydrogen refuelling infrastructure) from fuel cell electric vehicles (FCEVs). The test-case is used to verify the effectiveness of the proposed DR-integrated energy planning optimisation model.

2.1. Micro-grid equipment

For the purposes of this study, the leading brands of equipment in New Zealand's renewable energy asset market were chosen based on the first author's judgement of prevalence. The following sub-sections mathematically model the system equipment.

2.1.1. Photovoltaic plant

Canadian Solar's CS6K-280P poly-crystalline photovoltaic (PV) modules [48], which have a nominal power of 280 W are employed in this study for PV power generation. The power output from the PV plant at each time-step, $P_{PV}(t)$ [kW], can be estimated as follows [25,49,50]:

$$T_m(t) = T_a(t) + I_G(t) \times \frac{NMOT - 20}{0.8}, \tag{1}$$

$$P_{PV}(t) = N_{PV} \times P_{PV,r} \times \eta_{PV,DC/DC} \times DF \times \frac{I_G(t)}{I_{STC}} \times \left(1 - \frac{K_p}{100} \times (T_m(t) - T_{STC})\right), \tag{2}$$

where N_{PV} is the optimum quantity of the modules; $P_{PV,r}$ is the rated capacity of the module under the standard test conditions (STC); $\eta_{PV,DC/DC}$ is the PV plant's DC/DC converter efficiency; K_p is the temperature coefficient of the module; T_m, T_a, and T_{STC} respectively represent the PV module temperature, ambient temperature, and the module temperature at the STC; I_G and I_{STC} respectively denote the global solar irradiance on the horizontal surface and the solar irradiance at the STC; and *NMOT* and *DF* respectively stand for the nominal module operating temperature and derating factor. The tilt angle is assumed as 30° and the Meteonorm software [51] is used to normalise the values of I_G to this tilt angle. Also, the numeric values 20 and 0.8 respectively represent the ambient temperature [°C] and solar irradiance [kW/m^2] at which the *NMOT* is defined.

2.1.2. Wind plant

The wind turbine (WT) ECO 48/750, which has a rated power of 750 kW is considered for wind power generation [52]. The turbine's manufacturer-provided characteristic power-wind speed curve is shown in Fig. 3. The wind plant's output power at each time-step, $P_{WT}(t)$ [kW], can be obtained by multiplying the optimal quantity of the WTs, N_{WT}, by each turbine's output power estimated from the power curve presented in Fig. 3. Also, since the power curve of the WT is characterised for its hub height wind speed, Eq. (3) can be used to normalise the wind speed data measured at other heights to the turbine's hub height [53].

$$V_h = V_{ref} \times \left(\frac{h}{h_{ref}}\right)^{\gamma}, \tag{3}$$

where V_{ref} denotes the reference wind speed collected at the height of h_{ref} and $\gamma \in [0.1, 0.25]$ is the wind shear exponent, which varies with respect to the terrain [54].

2.1.3. Micro-hydro plant

Suneco Hydro's XJ50-100SCTF6-Z 100-kW micro-hydro turbines are selected to be integrated into the run-of-the-river plant as part of the MG system [55]. The power output from the plant at each time-step [kW] can be estimated from Eq. (4) [56,57].

$$P_{MH}(t) = \frac{N_{MH} \times \eta_{MH,AC/DC} \times \eta_{MH} \times \rho \times g \times h_g \times F(t)}{1000}, \tag{4}$$

where N_{MH} denotes the optimum quantity of turbines, η_{MH} is the total efficiency of the plant (including the turbine, generator, and water

[1] In game theory, a Stackelberg duopoly is a non-symmetric, strategic, sequential game with one party, or a group of parties, taking over the leading position and the other(s) acting as follower(s).

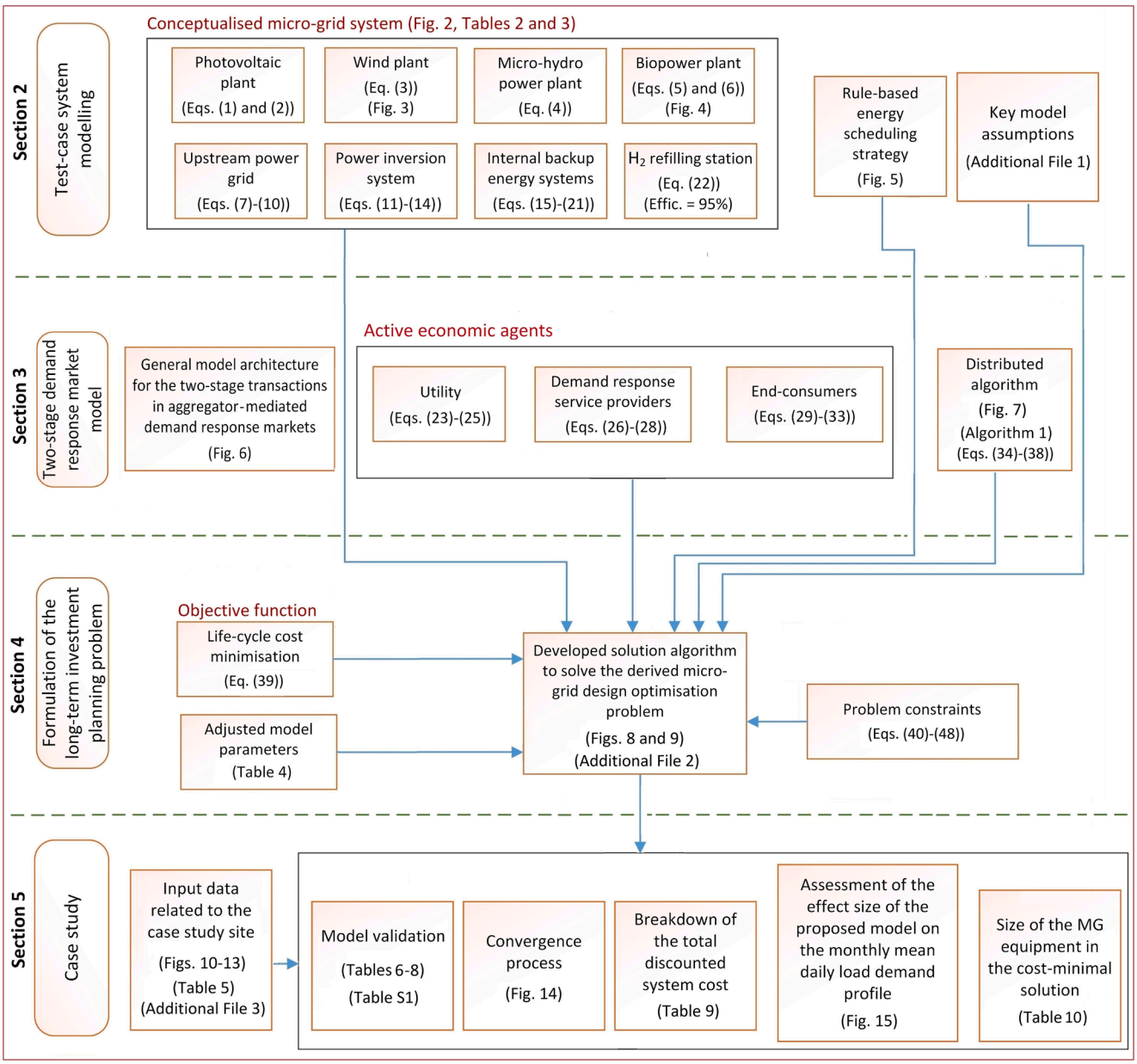

Fig. 1. Overview of the section-wise modelling procedure employed in this paper for the aggregator-mediated, market-driven integration of flexible demand resources in the long-term planning of MGs.

wheel efficiency), $\eta_{MH,AC/DC}$ is the efficiency of the plant's AC/DC converter, ρ represents the density of water, g is the acceleration due to gravity, h_g is the gross head (which is defined as the difference between the head race and tail race levels when water is not flowing), $F(t)$ is the flow rate at time-step t [m^3/s], while the numeric value of 1000 converts the unit of measurement from Wh to kWh.

2.1.4. Biomass plant

The integrated biomass gasifier-generator system PP30 Cogen-CS manufactured by All Power Labs [58] is utilised in this study. The plant, the flow diagram of which is shown in Fig. 4, is a commercially available, off-the-shelf component with an electrical rated power of 25 kW. The power output from the biomass plant at each time-step [kW] can be calculated from Eq. (5) [59].

$$P_{BP}(t) = N_{BP} \times \eta_{BP,AC/DC} \times \eta_{BP} \times CV \times M_{BP}(t), \quad (5)$$

where N_{BP} represents the optimal quantity of the considered biopower units, $\eta_{BP,AC/DC}$ is the efficiency of the plant's AC/DC converter, η_{BP} is the overall bio-electricity generation efficiency of the system, CV stands for the gross calorific value of the biomass feedstock, and $M_{BP}(t)$ denotes the feedstock mass consumption rate at time-step t [kg/h].[2]

Furthermore, the system is characterised with a carbon emission factor of 1.53 kg-CO_2 per kg of feedstock used [60]. Accordingly, the social cost of the carbon emissions needs to be factored into the decision-making–for an eco-design of the MG system. The following equation can be used to calculate the life-cycle penalty imposed on the MG for CO_2 emissions:

[2] Note that the rated powers of micro-hydro turbines and biopower plants, are incorporated into the model and the decision-making process in an indirect manner using the power rating-dependent parameters–h_g in the case of micro-hydro turbines, and M_{BP} in the case of biopower units–as well as specifically developed terminal constraints (refer to Section 4.2.6 for more details).

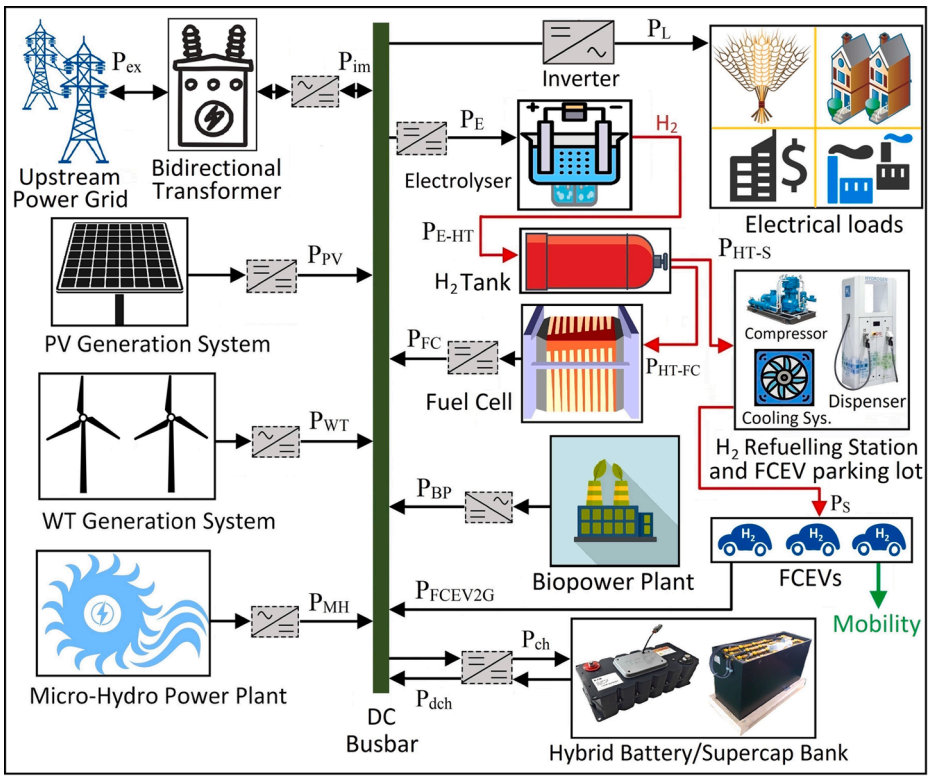

Fig. 2. Micro-grid system architecture and streams of energy driven by renewables and the upstream grid.

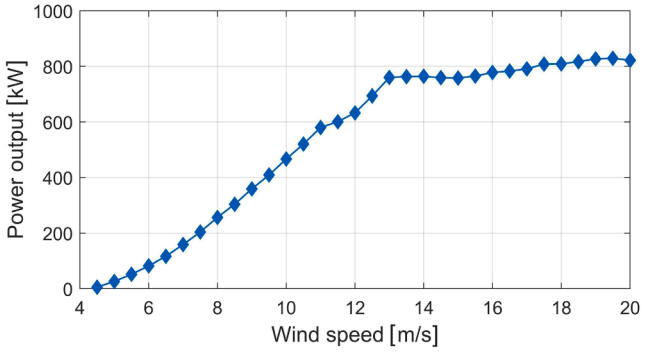

Fig. 3. Power curve of the ECO 48/750. Data Source: [52].

$$cost_{em} = \frac{\xi_{CO_2}}{1000} \times E_{CO_2} \times \sum_{t=1}^{T} M_{BP}(t), \tag{6}$$

where ξ_{CO_2} [\$/tCO$_2$] denotes the social cost of CO$_2$ emissions used as a reference to account for life-cycle GHG impacts of the biopower plant in the model, and E_{CO_2} represents the CO$_2$ emission factor of the plant [kg-CO$_2$/kg-feedstock].

2.1.5. Upstream power grid

The MG system is tied to the upstream electricity network through a dedicated bidirectional MV/LV transformer, the optimal capacity of which is under investigation. The cost imposed by purchasing electricity from the grid at each time-step could be represented by Eq. (7), while the income generated by the MG's electricity exports is obtained from Eq. (8) [61].

$$cost_{im}(t) = \pi_{im}(t) \times P_{im}(t) \times \Delta t, \tag{7}$$

$$income_{ex}(t) = \pi_{ex} \times P_{ex}(t) \times \Delta t, \tag{8}$$

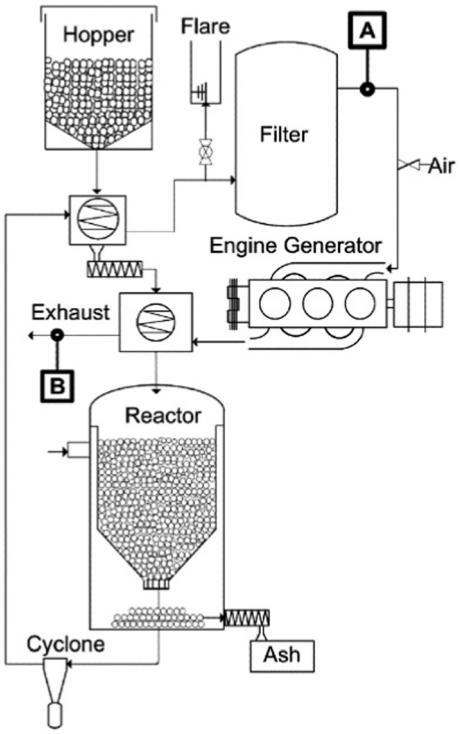

Fig. 4. Schematic diagram of the considered integrated biomass gasifier-generator system. Source: [60].

where $\pi_{im}(t)$ represents the (time-varying) wholesale electricity market price at time-step t [\$/kWh], π_{ex} is the utility grid's single-tier (flat) buy-back rate [\$/kWh], $P_{im}(t)$ is the amount of power imported from the utility grid at time-step t, $P_{ex}(t)$ is the amount of power exported to the

main grid at time-step t, and Δt represents the length of each time-step.

The power exchange is expected to adhere to the following constraints:

$$P_{im}(t)/\eta_T \leq N_T, \tag{9}$$

$$P_{ex}(t)/\eta_T \leq N_T, \tag{10}$$

where η_T denotes the transformer's efficiency and N_T represents the rated capacity of the transformer, which is to be optimised.

The generic solid-state transformer, designed by Qin and Kimball [62], is used in this study. The size of the transformer is characterised by the apparent power [kVA] and, as a simplifying assumption, the power factor is assumed to be 0.95.

2.1.6. Power conversion apparatuses

As shown in Fig. 2, the MG system is equipped with several converters to serve the purpose of coupling the equipment to a common DC busbar. For electrical loads, Leonics' GTP-519-S 900-kW, GTP-506 115-kW, and GTP-501 33-kW inverters are considered in this study [63]. To calculate the size of the electrical loads' inverters, first, the following equation is used to determine the nominal power of the overall power inversion system:

$$N_I = \frac{P_{L,max}}{\eta_I}, \tag{11}$$

where $P_{L,max}$ represents the demanded annual peak electrical loads and η_I identifies the power inversion equipment's efficiency.

Then, N_I is rounded up to the next integer and the number of each inverter model is identified by the following equations, which give priority to higher-rated inverters as they carry a lower per-unit cost:

$$N_{900} = \left\lfloor \frac{N_I}{C_{900}} \right\rfloor, \tag{12}$$

$$N_{115} = \left\lfloor \frac{N_I - (N_{900}C_{900})}{C_{115}} \right\rfloor, \tag{13}$$

$$N_{33} = \left\lceil \frac{N_I - (N_{900}C_{900}) - (N_{115}C_{115})}{C_{33}} \right\rceil, \tag{14}$$

where N_{900}, N_{115}, and N_{33} respectively denote the quantity of the 900-kW, 115-kW, and 33-kW inverters, while C_{900}, C_{115}, and C_{33} indicate their respective rated capacities.

2.1.7. Internal backup energy storage

The proposed system leverages the temporal characteristics of various DERs providing backup power, or energy storage. To this end, this study expands on the idea proposed by Akram et al. [64] that low-pass energy filters could be used to calculate the share of each energy storage medium in supplying load power demand on a representative MG. Accordingly, the power mismatch signal is first broken down into the low- and high-frequency components using a low-pass filter with a transfer function given in Eq. (15).

$$H(s) = \frac{K\omega_0^2}{s^2 + (\omega_0/Q)s + \omega_0^2}, \tag{15}$$

where ω_0 denotes the cut-off frequency, K represents the DC gain, and $Q = 1/2\xi$ identifies the quality with ξ indicating the damping factor.

Then, the low-frequency signal is directed to the hydrogen system (including the electrolyser, hydrogen tank, and the fuel cell), while the high-frequency signal is transferred to the hybrid battery-SC system. Subsequently, another low-pass filter with a lower cut-off frequency identifies the contribution of the battery and SC banks in serving loads or storing surplus power.

The technical rationale underlying this power allocation approach is the longer cycle life, higher round-trip efficiency, and more rapid response capability of SCs (batteries) to balance out generation-demand mismatches than batteries (the hydrogen system). That is, the shortest and longest periods of surplus or shortage of electricity are addressed using the SC bank and hydrogen system, respectively, while the battery bank bridges the gap between these two storage media.[3]

2.1.7.1. Super-capacitor bank. Eaton's 48-V, 166-F XLR-48R6167-R SC modules [65], which are of the type electrochemical double-layer capacitor (EDLC), are used to address short-term renewable power and load demand mismatches–and improve the MG's dynamic response and overall efficiency. The SC bank's energy content at each hour of the MG operation can be calculated as follows:

$$E_{SC}(t) = E_{SC}(t-1) + \left(P_{ch,HF2} - \left(\frac{P_{dch,HF2}}{\eta_{SC}} \right) \right) \times \Delta t, \tag{16}$$

where η_{SC} represents the SC's round-trip efficiency, while $P_{ch,HF2}$ and $P_{dch,HF2}$ are the high-frequency components of the outputs of the second-stage filtered charging and discharging signals, respectively.

2.1.7.2. Battery bank. CellCube's vanadium redox flow-based battery bank [66] is used in the conceptualised MG. Likewise to the inverter system, three different battery product models are selected and the same procedure is followed to apportioning the total optimal size of the battery bank to different model types, following the same logic. The battery product models are: FB 10–100 (100 kWh), FB 200–400 (400 kWh), and FB 400–1600 (1600 kWh). The battery bank's energy content at each hour can be obtained as follows:

$$E_B(t) = E_B(t-1) + \left(P_{ch,LF2} - \left(\frac{P_{dch,LF2}}{\eta_B} \right) \right) \times \Delta t, \tag{17}$$

where η_B is the battery bank's round-trip efficiency, while $P_{ch,LF2}$ and $P_{dch,LF2}$ denote the low-frequency components of the outputs of the second-stage filtered charging and discharging signals, respectively.

2.1.7.3. Hydrogen storage. The hydrogen-based storage system mainly includes polymer electrolyte membrane (PEM) electrolyser stacks, a medium-pressure (20 bar) hydrogen reservoir, and stationary PEM fuel cell stacks. H-TEC Systems' S 30/50 5-kW electrolyser stacks [67], a generic hydrogen reservoir (which needs to be customised), and Ballard's FCgen-1020ACS 3.3-kW fuel cell stacks [68] are used as part of the hydrogen storage system. The hydrogen power directed from the electrolyser outlet to the reservoir at time-step t can be obtained as follows:

$$P_{E-HT}(t) = P_E(t) \times \eta_E, \tag{18}$$

where P_E is the electrolyser's consumed power, which is controlled by the low-frequency component of the output of the first-stage filtered charging signal, while η_E denotes the electrolyser's efficiency.

The mass of hydrogen, m_{HT} [kg], stored in the reservoir at each time-step can be calculated as follows:

$$E_{HT}(t) = E_{HT}(t-1) + \left(P_{E-HT}(t) - \frac{(P_{HT-FC}(t) + P_{HT-S}(t))}{\eta_{HT}} \right) \times \Delta t, \tag{19}$$

$$m_{HT}(t) = \frac{E_{HT}(t)}{HHV_{H_2}}, \tag{20}$$

where E_{HT} represents the reservoir's energy level, P_{E-HT} is the directed

[3] Note that the backup power allocation strategy employed in this study is tailored towards long-term capacity planning, at which stage long-term forecasted data are available. A forward-looking predictive modelling approach (using a critic network, for example) is indispensable for the real-time operation phase.

hydrogen power from the electrolyser to the reservoir, P_{HT-FC} and P_{HT-S} respectively denote the hydrogen power consumption of the fuel cell and the FCEV parking lot, η_{HT} represents the tank's round-trip efficiency, and HHV_{H_2} stands for the higher heating value of hydrogen.

The electric power output from the high-energy-density fuel cell at time-step t, which is controlled by the low-frequency component of the output of the first-stage filtered discharging signal, can be obtained using Eq. (21).

$$P_{FC}(t) = P_{HT-FC}(t) \times \eta_{FC}, \tag{21}$$

where P_{HT-FC} represents the fuel cell's consumed hydrogen power and η_{FC} denotes its electrical efficiency, which is defined as the ratio between the electricity generated and the hydrogen consumed.

2.1.8. Fuel cell electric vehicle parking lot

The hydrogen refuelling infrastructure of the parking lot mainly consists of a medium-pressure (20/350 bar) compressor, a buffer storage, a cryogenic pump, as well as a vaporiser, a refrigeration unit, and some dispensers to deliver gaseous hydrogen fuel to FCEVs [69]. The refuelling infrastructure is modelled by its overall efficiency, which is denoted by η_S. To this end, the Pure Energy Centre's customised hydrogen refilling station [70] is considered for integration into the proposed MG.

2.1.8.1. Selected fuel cell electric vehicles. A fleet of ultra-light-duty personal passenger vehicles is planned for integration into the envisioned system through the coordinated use of the refuelling infrastructure. Accordingly, vehicles are assumed to be refuelled on a first-come/first-served basis using the multi-server Erlang-C queuing model [71], where C identifies the optimal number of dispensers. Also, FCEVs are assumed to be of the model Riversimple Rasa.

2.1.8.2. Fuel cell electric vehicles in vehicle-to-grid operation. To provide a platform for exploiting the V2G capabilities of the FCEVs, the FCEV2G setup designed in [72] is used in this study. The setup enables the conversion of the DC power of the vehicle's fuel cell engine into AC that can be directed to the input port of the electrical loads' inverter after frequency synchronisation, with an overall efficiency of η_{FCEV2G}. Accordingly, modulation of the power output from each FCEV, the owner of which aspires to participate in the V2G operations, can be made from 0 to 8.5 kW DC–in compliance with the nominal capacity of Rasa's built-in fuel cell. This means the costs arising from payments made to FCEV owners to provide V2G power at each time-step–under a feed-in-tariff style programme–can be calculated by the following equation:

$$cost_{FCEV2G}(t) = \pi_{FCEV2G} \times \eta_{FCEV2G} \times P_{FCEV2G}(t) \times \Delta t, \tag{22}$$

where π_{FCEV2G} represents the per-unit premium tariff rate for V2G power [$/kWh] and $P_{FCEV2G}(t)$ denotes the amount of V2G power used for operational scheduling at time-step t.

For the sake of simplification, it was assumed that at each time-step of the MG operation, the maximum amount of available V2G power that can be provided by the station at each time-step, $P^{max}_{FCEV2G}(t)$, equals 25% of the load reduction potential of the station at that time-step.

2.1.9. Data: Selected product models

The values of the underlying system scalars, defined above, are presented in Table 2. Also, the techno-economic specifications of the MG equipment, namely the capital, replacement, and operation and maintenance (O&M) costs, as well as the estimated service life and efficiency of the equipment are summarised in Table 3.

2.2. Operational strategy

A rule-based, hourly-basis, cycle-charging operational strategy is adopted in this study for the dispatch of energy within the MG system, which is illustrated by the flowchart in Fig. 5. In the devised energy scheduling plan, (1) energy storage devices and FCEVs are recharged/refilled using only the surplus non-dispatchable renewable power, (2) non-dispatchable renewable power and electrical loads are partitioned into the ultra-high, high, and low-frequency components and then stored/supplied within/using the SC bank, battery bank, and the hydrogen tank/fuel cell, respectively, (3) the dispatchable biopower plant can only be operated during the time-slots stamped as peak hours to partially or wholly offset the lack of sufficient fuel cell power,[4] (4) the upstream grid serves as the ultimate guarantor of the perfect satisfaction of the electric load demand, and (5) the FCEV2G capability is considered as a resource to compensate for at least part of the electricity left unserved by the fuel cell and the biopower plant, or the shortage of battery and SC capacity to meet the load power demand. To this end, morning and evening peak demand were assumed to occur between the hours of 6 a.m. to 10 a.m. and 5 p.m. to 9 p.m., respectively–in compliance with historical records of electricity consumption in New Zealand.

Moreover, the key assumptions made in conceptualising the proposed MG system and conducting the life-cycle analysis are listed in Supplementary Material (Additional File 1: Key assumptions underlying the conceptualised micro-grid model).

Table 2
Data values and sources for the proposed micro-grid system scalars.

Scalar	Value	Source	Scalar	Value	Source
CV	5.07 kWh/kg	[73]	K_p	−0.40%/°C	[48]
Δt	1 h	(this paper)	$NMOT$	43 °C	[48]
$\eta_{PV,DC/DC}$	95%	[34]	ρ	1000 kg/m^3	–
$\eta_{MH,AC/DC}$, $\eta_{BP,AC/DC}$	95%	[34]	$P_{BP,r}$	25 kW	[58]
DF	85%	[74]	π_{ex}	$0.05/kWh	[75]
E_{CO_2}	1.53 kg-CO_2/kg-feedstock	[60]	π_{FCEV2G}	$0.05/kWh	(this paper)
g	9.81 m/s^2	–	$P_{L,max}$	7.31 MW	(this paper)
h	55 m	[52]	$P_{MH,r}$	100 kW	[55]
h_g	10 m	[55]	$P_{PV,r}$	0.28 kW	[48]
h_{ref}	10 m	[76]	T_{STC}	25 °C	[78]
HHV_{H_2}	39.7 kWh/kg	[77]	γ	0.15	[79]
I_{STC}	1 kW/m^2	[78]	ξ_{CO_2}	$42/tCO$_2$, $50/tCO$_2$*	[80]

* A central value of $42/tCO$_2$ is applied for the first 10-year planning horizon (covering the years 2020 to 2030), which rises to $50/tCO$_2$ for the second half of the projected lifespan of the project in accordance with the Obama administration's central estimates [80].

3. Aggregator-mediated, incentive-based demand-side management market design

This section presents a mathematical formulation of a two-stage, aggregator-mediated, incentive-based DSM market model specifically developed for integration into standard MG capacity planning approaches. Building on the interruptible load programmes, the model is designed specifically to improve the accuracy of projections of the small- to medium-scale DR resource availability across different end-use sectors–residential, commercial, industrial, agricultural, and electrified transportation. More specifically, it characterises the interactions between a MG operator, DRAs, and end-consumers. To this end, the model consistently treats these three sets of actors as rational, utility-

[4] This assumption can be explained by the relatively long cold start-up time of the biopower plant (i.e. ~10–15 min) and the inefficiency of leaving the biopower plant on standby at all times.

Table 3
Data values and sources for techno-economic specifications of the conceptualised system's components.

Component	Manufacturer part number	Nameplate rating	Capital cost*		Replacement cost†	Operation and maintenance cost†	Expected service life	Nominal efficiency		Source
			Per unit	Per standard unit of generation/ storage/ conversion capacity				Notation	Value [%]	
PV module	CS6K-280P	280 W	$210/ unit	$750/kW	$200/unit	$1/unit/year	25 years	η_{PV}	17.11	[48]
Wind turbine	ECO 48/750	750 kW	$1.096 m/unit	$1.46 k/kW	$0.822 m/ unit	$21 k/unit/ year	20 years	N/A‡	N/A‡	[52]
Micro-hydro turbine	XJ50-100SCTF6-Z	100 kW	$56 k/ unit	$560/kW	$17 k/unit	$2 k/unit/year	25 years	η_{MH}	78	[55]
Biopower unit§	PP30 Cogen-CS	25 kW	$32 k/ unit	$1.28 k/kW	$23 k/unit	$0.01/unit/ hour	10 k hours	η_{BP}	23	[58]
Transformer	Generic	–	–	$65/kVA	$55/kVA	$2/kVA/year	30 years	η_T	93	[62,81]
Inverter	GTP-501	33 kW	$12 k/ unit	$364/kW	$12 k/unit	$85/unit/year	15 years	η_I	96	[63]
	GTP-506	115 kW	$38 k/ unit	$330/kW	$38 k/unit	$250/unit/ year				
	GTP-519-S	900 kW	$270 k/ unit	$300/kW	$270 k/unit	$1.9 k/unit/ year				
Super-capacitor module	XLR-48R6167-R	166F, 48 V ≡ 0.054 kWh	$1.3 k/ unit	$24.1 k/kWh	$1.3 k/unit	$13/unit/year	1 m cycles	η_{SC}	97	[65]
Battery pack	FB 10–100	100 kWh	$110 k/ unit	$1.1 k/kWh	$110 k/unit	$220/unit/ year	20 years with unlimited cycles	η_B	80	[66,82]
	FB 200–400	400 kWh	$400 k/ unit	$1 k/kWh	$400 k/unit	$840/unit/ year				
	FB 400–1600	1600 kWh	$1.442 m/unit	$901/kWh	$1.442 m/ unit	$4 k/unit/year				
Electrolyser stack	S 30/50	5 kW	$6 k/ unit	$1.2 k/kW	$6 k/unit	$120/unit/ year	20 years	η_E	75	[67]
Hydrogen tank	Generic	–	–	$500/kg	$500/kg	$1/kg/year	20 years	η_{HT}	95	[83]
Fuel cell stack	FCgen-1020ACS	3.3 kW	$5 k/ unit	$1.52 k/kW	$5 k/unit	$0.02/unit/ hour	10 k hours	η_{FC}	40	[68]
Hydrogen station	Generic (Pure Energy Centre)	–	–	$10 k/(kg-$H_2$/h)	$5 k/(kg-$H_2$/ h)	$350/(kg-$H_2$/ h)/year	20 years	η_S	95	[69,70,84]
	Generic (The Energy Technology Section, TU Delft)¶‖	–	–	$155/kW	$95/kW	$32/kW/year	20 years	η_{FCEV2G}	44#	[85,86,87,88]

¶ In view of the assumption that the DC power provided by the FCEVs is fed into the electrical loads' inverter, the costs associated with the FCEV2G technology only include the costs of modifying the vehicles with a V2G DC outlet plug.

* All of the reported capital costs represent the actual cost of buying the selected components in New Zealand's energy asset market as of October 2019–which were adjusted to 2019 U.S. dollars. In October 2019, US$1 = NZ$1.56.

† All of the replacement and O&M costs were calibrated in accordance with the component-specific ratios of capital to replacement and O&M costs reported in [82,83,89,90,91,92,93,94,95].

‡ Not applicable as the wind turbine efficiency is reflected in its power curve shown in Fig. 3.

§ To value the positive impact of the biopower plant on the internal dispatchability of the MG, the total discounted cost of pellet feedstock was considered to be an exogenous variable, which is determined outside the model based on the imposed emission credits (see Eq. (6)) with respect to the total discounted energy output of the plant (see Eq. (5)).

The V2G infrastructure's efficiency in this paper represents a tank-to-DC-bus efficiency (units converted based on the higher heating value of hydrogen).

maximising (self-interested), active economic agents. The proposed market design provides a forum for these economic agents to negotiate on how to mutually optimise their objective functions in non-cooperative (strategic) game settings under the Stackelberg competition. It also identifies the minimum operational MG costs based on hourly priced DR products and the wholesale power price. In this way, the model enables all the active agents within the MG to be involved in co-designing a business model for more independent energy procurement. Fig. 6 displays a schematic of the overall structure of the model with the sequence of incentive price/DR supply communications between the market participants overlaid [96].

As Fig. 6 shows, the market-based, aggregator-mediated DSM strategy is modelled as an interactive hierarchical decision-making process, which consists of two levels of leader–follower relationships, namely between the MG operator and the DRAs (wholesale DSM market), and between the DRAs and their customers (retail DSM market). Although the DSM market participants are hierarchically related with respect to DR service, each has an independent viewpoint on the problem, which is modelled by specific objective functions in the following sub-sections.

3.1. Micro-grid operator

It is assumed that the conceptualised MG, laid out in Section 2, runs on an energy-as-a-service business model in that not only does a third-party (private company) own the MG, but it also provides an overarching framework for energy management (through effective incentive

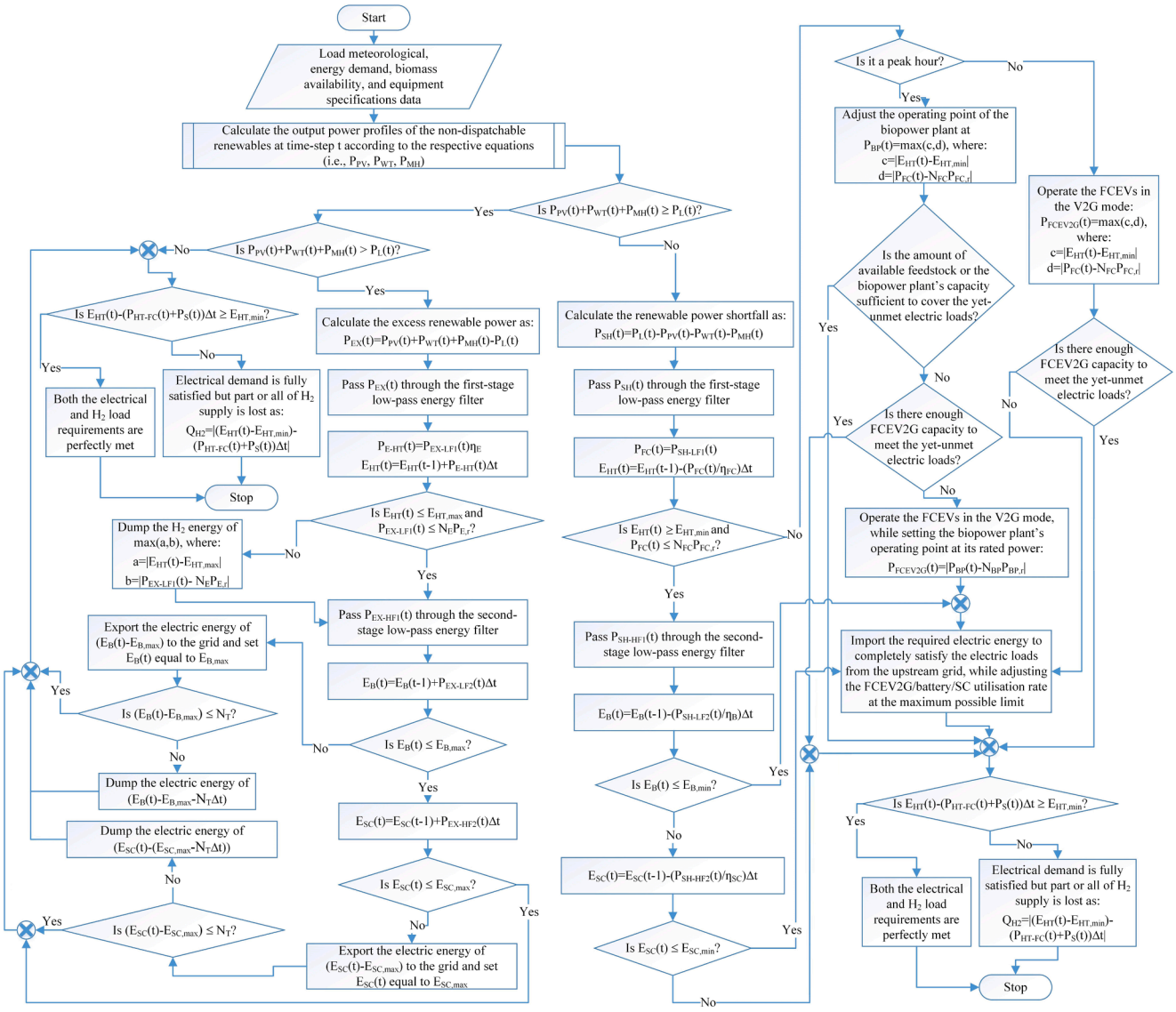

Fig. 5. Flowchart of the MG's energy management scheme, consisting of a set of pre-defined control logics.

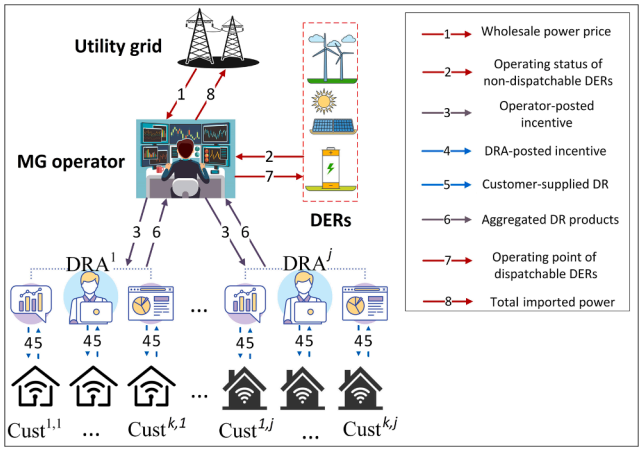

Fig. 6. General architecture of the proposed two-stage, aggregator-mediated, incentive-based DSM market design.

arrangements reflective of wholesale market prices) tailored to the needs of the MG.

Specifically, on a 24-h day-ahead basis, the MG operator predicts the net energy deficit of the MG, which needs to be procured by a combination of imported power and customer-supplied DR units. Accordingly, it sends an incentive payment signal to the aggregators to induce lower energy use at times of high wholesale power prices, when the total power output from the renewable power generation technologies is low, or during periods when reserve shortfalls arise. Equation (23) expresses the objective function of the MG operator, which needs to be minimised for each critical hour of the next day ($t \in P_d \subset T = \{1,2,\cdots,8760\}$) subject to the constraints in Eqs. (24) and (25):

$$OC_{MG}(t) = cost_{im}(t) + I_{MGO}(t) \times \sum_{j \in J} D^j_{LA}(t) \forall t, \tag{23}$$

$$I^{min}_{MGO} \leq I_{MGO}(t) \leq I^{max}_{MGO} \forall t, \tag{24}$$

$$D_{def}(t) = P_{im}(t) + \sum_{j \in J} D^j_{LA}(t) \forall t, \tag{25}$$

where OC_{MG} is the MG's operational cost defined based on the cost of the imported power, $cost_{im}$, and the total incentive payments for load

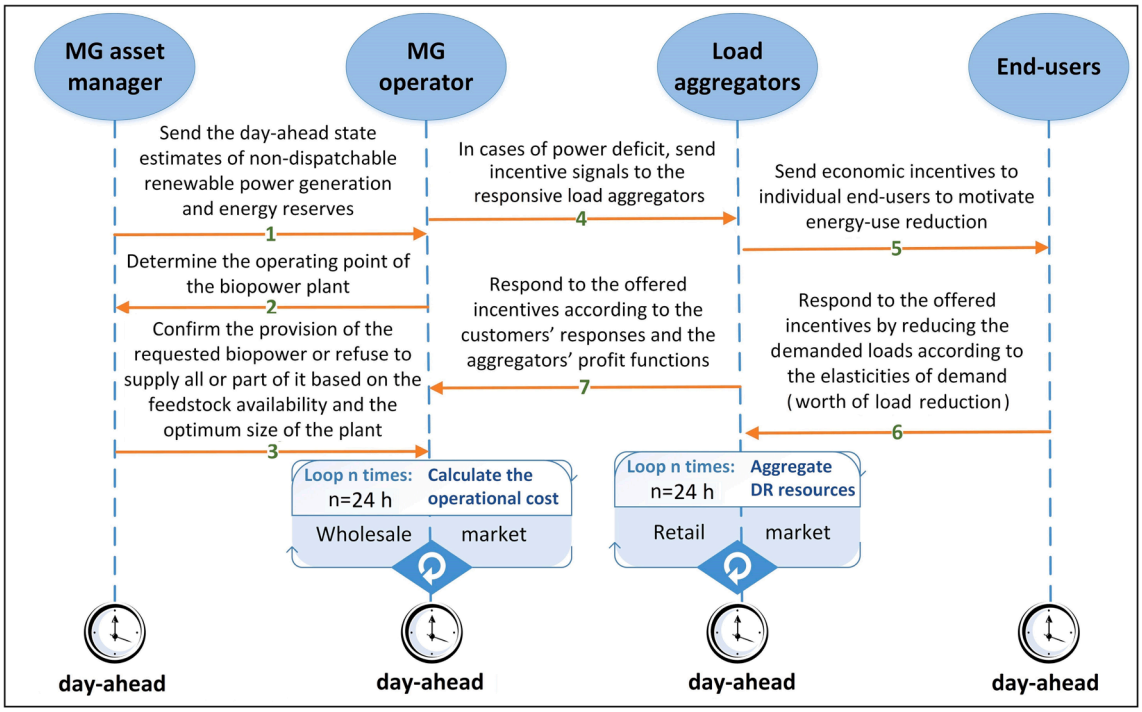

Fig. 7. Sequence diagram of implementing the proposed DSM model in the context of the conceptualised MG system.

reduction, $\sum_{j\in J} D^j_{LA}$; I_{MGO} is the MG operator-posted incentive price signal to the wholesale DSM market, with superscripts *min* and *max* representing its lower and upper limits, respectively; D_{def} denotes the net energy deficit of the system; and D^j_{LA} is the total load reduction procured by DRA $j \in J$.

3.2. Demand response aggregators

The DRAs serve as a go-between, interfacing with the smaller DR providers and the broader MG system operator so as to maintain the visibility of the small-scale DR products. The independence of the DRAs is fully preserved in the proposed model as they are precluded from ownership of the energy infrastructure. Precisely, third-party aggregators enlist end-consumers to take part in interruptible load programmes. To this end, they take a percentage of the MG operator-offered incentive as compensation, passing the rest on to their customers. More specifically, the DRAs aim to maximise the objective (profit) function in Eq. (26) subject to the constraints in Eqs. (27) and (28) [97]:

$$Pr^j_{LA}(t) = \left(I_{MGO}(t) - I^j_{LA}(t)\right) \times D^j_{LA}(t) \forall j, t, \tag{26}$$

$$I^{j,min}_{LA} \le I^j_{LA}(t) \le I^{j,max}_{LA} \forall j, t, \tag{27}$$

$$D^j_{LA}(t) = \sum_{k\in N_j} d^{k,j}(t) \forall j, t, \tag{28}$$

where I^j_{LA} is the incentive rate posted by the j-th aggregator to the retail DSM market; $d^{k,j}$ denotes the capacity of DR product supplied by customer k subscribed to aggregator j; N_j is the set of customers serviced by aggregator j, which is a proper subset of set of all the customers within the MG system's operational territory, K; and $I^{j,min}_{LA}$ and $I^{j,max}_{LA}$ respectively represent the lower and upper bounds of the incentive payments offered by aggregator j.

3.3. End-consumers

End-consumers, who are activated by third-party DRAs, have the opportunity to take full advantage of their flexibility potential, whilst adhering to a set of discomfort cost constraints. To this end, the end-consumers determine the optimum supply of their DR resources with respect to the DRA-offered incentive prices by maximising the utility function expressed in Eq. (29) subject to Eqs. (30) and (31).

$$U^{k,j}(t) = d^{k,j}(t) \times I^j_{LA}(t) - dis^{k,j}(t) \forall k, t, \tag{29}$$

$$0 \le d^{k,j}(t) \le d^{k,j}_{ncr}(t) \forall k, t, \tag{30}$$

$$d^{k,j}_{full}(t) = d^{k,j}_{cr}(t) + d^{k,j}_{ncr}(t) \forall k, t, \tag{31}$$

where $dis^{k,j}$ denotes the cost of discomfort (inconvenience) associated with load reductions as a measure of the value of electricity, which can be obtained from Eq. (32)[5] [98,99], and must lie within a certain range, as constrained by Eq. (33); $d^{k,j}_{full}$ is the full (original) load demanded by customer k of aggregator j; $d^{k,j}_{cr}$ is the critical portion of the original load, any shedding of which results in impaired reliability; and $d^{k,j}_{ncr}$ is the non-critical (dispatchable) demand, which can be interrupted by making effective incentive payments to customers for curtailing load.

$$dis^{k,j} = c^{k,j}_1 (d^{k,j})^2 + c^{k,j}_2 (1-\delta_j) d^{k,j} \forall k, t, \tag{32}$$

$$dis^{k,j,min} \le dis^{k,j} \le dis^{k,j,max} \forall k, t, \tag{33}$$

where $c^{k,j}_1$ and $c^{k,j}_2$ are positive individual-level parameters specified by end-consumers that characterise their sensitivity to load reductions, for customers indifferent to incentive payment, $c^{k,j}_1, c^{k,j}_2 \to \infty$; $0 \le \delta_j \le 1$ is the sector-level elasticity of customer-supplied DR capacity, for a hypothetical completely inelastic customer category, $\delta_j \to 0$; while $dis^{k,j,min}$ and $dis^{k,j,max}$ respectively denote the minimum and maximum allowable

[5] The customer discomfort cost function can be viewed as the second-order best-fit equation to individual-level, user-specified data points representing ordered pairs of DR capacity supply and the associated discomfort cost incurred.

limits for customer-specific discomfort costs.

Incorporating the term $(-c_2^{k,j}\delta_j d^{k,j})$ in Eq. (32) ensures that the market equilibrium of the two-stage aggregator-mediated DSM game is aware of the marginal values the end-users across different sectors place on an uninterrupted power supply–that is, the value to consumers of the last (incremental) unit of DR capacity supply. It should be noted that this analysis does not account for the supply elasticity of inframarginal DR capacity.

3.4. Solution algorithm

To solve the proposed two-stage, aggregator-mediated, incentive-based DSM market model, a distributed algorithm approach, which dynamically updates the MG operator-offered incentive price, is implemented. The idea is to update the MG operator-posted incentive from I_{MGO}^{min} to I_{MGO}^{max} with an increment size of i_{MGO} and determine the hourly operational cost of the MG as a function of the wholesale power price and contributed load reductions. The model is solved repeatedly for different values of the MG operator-offered incentive prices until no further improvement (reduction) in the MG operational cost occurs (terminating condition). Algorithm 1 presents the distributed algorithm developed to quantify the optimal trade-off between the imported power and dispatched load reduction during the critical hours of MG operation in terms of on-site resource adequacy. The superscript "*" in the algorithm denotes the global optimality.

Algorithm 1. (*Proposed distributed algorithm to produce the optimal day-ahead trade-offs between imported power and exploited DR resources during the critical peak hours of MG operation*)

1: Initialise: $I_{MGO}^{*}=0$ and $OC_{MG}^{*}(t)=cost_{im}(D_{def})$
2: **for** I_{MGO} ranging from I_{MGO}^{min} to I_{MGO}^{max} at steps of i_{MGO} **do**
3: Submit the incentive price signal I_{MGO} to the wholesale DSM market
4: **for** each DRA $j \in J$ **do**
5: Determine the best-strategy incentive rate to be offered to the end-users, $I_{LA}^{j,*}$, by setting the first-order derivative of the DRA's profit function in Eq. (26), in which $d^{k,j}$ is substituted with the best-response strategy of the corresponding customers derived by setting the first-order derivative of their utility functions in Eq. (29) equal to zero
6: Send the incentive price signal $I_{LA}^{j,*}$ to the corresponding customers
7: **for** each customer $k \in N_J$ **do**
8: Derive the customer's best-response strategy by setting the first-order derivative of its utility function given in Eq. (29) equal to zero
9: Calculate the best-response load reduction with respect to the financial incentive offered by the DRA it has subscribed to, using the customer-specific best-response strategy profile derived above
10: Send the amount of load curtailment contributed by the customer to the corresponding DRA
11: **end for**
12: Aggregate the load reductions supplied by the end-users
13: Send the total load reduction procured by the DRA to the MG operator
14: **end for**
15: Update the hourly operating cost of the MG as:
$OC_{MG}=cost_{im}\left(D_{def}-\sum_{j\in J}D_{LA}^{j}\right)+I_{MGO}\times\sum_{j\in J}D_{LA}^{j}$
16: **if** $(OC_{MG}<OC_{MG}^{*})$ **then**
17: Update the optimal MG operator-posted incentive and the MG's operating cost as: $I_{MGO}^{*}=I_{MGO}$ and $OC_{MG}^{*}=OC_{MG}$
18: **end if**
19: **end for**
20: Return the set $(I_{MGO}^{*}, I_{LA}^{j,*}, d^{k,j,*})$ as the unique, globally-optimum equilibrium solution for each hour of the coming day

Algorithm 1 determines the unique, pure-strategy Nash equilibrium of the game, which identifies the best-response strategies of the DRAs and end-consumers by setting the first-order derivatives of their objective functions equal to zero. To prove that doing so maximises the customers' utility functions and the aggregators' profit functions (and yields the unique, globally-optimum solutions), one must show the concavity or convexity of these payoff functions.

Taking the second-order derivative of $U^{k,j}$ given in Eq. (29) with respect to the customer-supplied DR capacity yields:

$$\frac{\partial U^{k,j}}{\partial d^{k,j}}=I_{LA}^{j}-\left(2c_1^{k,j}d^{k,j}+c_2^{k,j}\left(1-\delta_j\right)\right), \tag{34}$$

$$\frac{\partial^2 U^{k,j}}{\partial\left(d^{k,j}\right)^2}=-2c_1^{k,j}. \tag{35}$$

Substituting the best-response strategies of end-consumers–obtained by setting the first-order derivative of their utility function, derived in Eq. (34), equal to zero–into the profit function of the DRAs given in Eq. (26), yields:

$$\begin{aligned}Pr_{LA}^{j}&=\left(I_{MGO}-I_{LA}^{j}\right)\times\sum_{k\in N_J}\frac{I_{LA}^{j}-c_2^{k,j}\left(1-\delta_j\right)}{2c_1^{k,j}}\\&=-\left(I_{LA}^{j}\right)^2\sum_{k\in N_J}\frac{1}{2c_1^{k,j}}+I_{LA}^{j}\left(\sum_{k\in N_J}\frac{c_2^{k,j}\left(1-\delta_j\right)}{2c_1^{k,j}}\right.\\&\quad\left.+\sum_{k\in N_J}\frac{I_{MGO}}{2c_1^{k,j}}\right)+I_{MGO}\sum_{k\in N_J}\frac{-c_2^{k,j}\left(1-\delta_j\right)}{2c_1^{k,j}}.\end{aligned} \tag{36}$$

Then, the second-order derivative of Pr_{LA}^{j}, re-written in Eq. (36), with respect to the aggregator-offered incentive payments can be obtained as follows:

$$\frac{\partial Pr_{LA}^{j}}{\partial I_{LA}^{j}}=-I_{LA}^{j}\sum_{k\in N_J}\frac{1}{c_1^{k,j}}+\left(\sum_{k\in N_J}\frac{c_2^{k,j}\left(1-\delta_j\right)}{2c_1^{k,j}}+\sum_{k\in N_J}\frac{I_{MGO}}{2c_1^{k,j}}\right), \tag{37}$$

$$\frac{\partial^2 Pr_{LA}^{j}}{\partial\left(I_{LA}^{j}\right)^2}=-\sum_{k\in N_J}\frac{1}{c_1^{k,j}}. \tag{38}$$

Given the positive value of $c_1^{k,j}$, the second-order derivatives of Pr_{LA}^{j} and $U^{k,j}$ are strictly negative. This implies that Pr_{LA}^{j} and $U^{k,j}$ are strictly concave over the feasible regions of I_{LA}^{j} and $d^{k,j}$, respectively. Accordingly, this proves that setting the first-order derivatives of the aggregators' and end-consumers' objective functions equal to zero is guaranteed to yield the unique, globally-optimum solutions.

3.5. Communication sequence

Furthermore, to help visualise the sequence of actions and reactions required to execute the proposed interruptible DR market design, the application-driven sequence diagram of Algorithm 1 is presented in Fig. 7 for the conceptualised MG, laid out in Section 2. As illustrated in the figure, the process starts by communicating the day-ahead state estimates of non-controllable renewables and energy reserves from one utility-owned entity, the MG asset manager, to another utility-owned entity, the MG operator. After receiving a response to its enquiry regarding the availability of biomass resources from the MG asset manager, the MG operator sends financial incentive signals to the DR aggregators and asks about the amount of available interruptible loads at each hour of the upcoming day. To this end, a two-stage iterative Stackelberg incentive price game is run in accordance with Algorithm 1, which enables decentralised decision-making. Specifically, at the top level (wholesale market), the MG operator is the leader and the DRAs are the followers. The DRAs are, at the same time, the leading players at the bottom level (retail market), where end-consumers serve as final followers. Note that the MG operator calls a DR event and sends the incentive price signals to the aggregators for the time-steps at which a net energy deficit is predicted.

The proposed DR scheduling framework, shown in Fig. 7, forms part of the input to the hourly energy management strategy of the proposed equipment capacity-planning method, the flowchart of which is provided in Fig. 5. That is, the energy demand data input to the flowchart is aware of the interruptible demand resources–or, better put, both the

power and hydrogen demand on the system are scaled-down (modified) through running the proposed DR scheduling framework for the specific peak hours of each day of the representative year before being fed to the hourly operational scheduling strategy outlined in Fig. 5. The process continues by transmitting the aggregator's incentives for load reduction to their corresponding customers, and completes by clearing the DSM markets respectively at the local (retail) and wholesale levels. As mentioned above, this procedure is repeated for each hour of a representative hourly-basis, one-year operational timeframe. To this end, the year-long demand profiles are decomposed into daily profiles so as to be used in the day-ahead DR management plan of the MG (see Fig. 7), the DR-adjusted values of which are then used in the course of the hourly energy management of the system (see Fig. 5).

4. Micro-grid capacity-optimisation model

This section explains the deterministically estimated life-cycle cost of the conceptualised MG system before describing how the proposed non-cooperative game-theoretic DR management scheme is integrated into the MG sizing model. The MG capacity-optimisation model consists of three key elements: (1) the net present cost (NPC) and net present value (NPV) methods utilised to formulate the total discounted system cost function, (2) the loss of power supply probability (LPSP) technique to quantify the reliability of the system in servicing the electrical and hydrogen load demands, and (3) the moth-flame optimisation algorithm (MFOA) [100] as a single-objective *meta*-heuristic optimisation algorithm to find the globally optimum solution to the problem by minimising the life-cycle cost of the MG, whilst adhering to the technical, reliability, and systemic constraints (see Supplementary Material (Additional File 2: Techniques used in the micro-grid capacity-optimisation model) for details). The superiority of the single-objective MFOA to the well-established *meta*-heuristics in the MG investment planning literature–for instance, the genetic algorithm (GA) [101] and the PSO [102]–as well as to a wide variety of state-of-the-art *meta*-heuristics in terms of nearing the globally optimum solution is supported in previous studies [41,84,103,104,105].

4.1. Objective function

A static analysis of expected future cash flows for the underlying project lays the basis for the mathematical formulation of the objective function. The whole-life cost of the MG based on the NPC and NPV calculations, which is to be minimised, can be expressed as follows:

$$\begin{aligned}\min WLC =&\left(\sum_{c\in C} NPC_c\right) + NPC_I + NPV\left(\sum_{t=1}^{8760} OC_{MG}(t)\right)\\ &+ NPV\left(\sum_{t=1}^{8760} cost_{em}(t)\right) + NPV\left(\sum_{t=1}^{8760} cost_{FCEV2G}(t)\right)\\ &- NPV\left(\sum_{t=1}^{8760} income_{ex}(t)\right) + pen_{const},\end{aligned} \tag{39}$$

Where NPC_c represents the NPC of the components, the optimal size of which is under investigation and are indexed by $c \in C = \{PV, WT, MH, T, E, FC, HT, BP, B, SC, S, FCEV2G\}$; NPC_I denotes the NPC incurred by the inverter; OC_{MG} is the operational cost of the MG to serve the unmet loads, either by paying incentives for load reduction or purchasing power from the upstream grid, as defined in Eq. (7); $cost_{em}$ is the cost imposed on the system for buying emission credits on account for running the biopower plant, as given in Eq. (6); $cost_{FCEV2G}$ denotes the cost resulting from the provision of FCEV2G services, as expressed in Eq. (22); $income_{ex}$ is the income generated by selling the surplus power to the main grid, as expressed in Eq. (8); while the term pen_{const} enforces the solutions to meet the constraints set out in Section 4.2.

In this context, the useful life of the project was considered to be 20 years and the real interest rate was set to 3.7%. The real interest rate was projected by taking the mean of the historical records in New Zealand over a 10-year period, between 2010 and 2019 [106].

4.2. Problem constraints

The objective function presented above is subject to various sets of constraints along the following lines.

4.2.1. System reliability

The LPSP reliability metric is employed to characterise the system performance over its projected 20-year life span. To this end, two separate LPSP indices are used to evaluate the reliability of electricity and hydrogen supply, which are constrained by Eqs. (40) and (41), respectively.

$$LPSP_e \le LPSP_e^{max}, \tag{40}$$

$$LPSP_{H_2} \le LPSP_{H_2}^{max}, \tag{41}$$

where $LPSP_e^{max}$ and $LPSP_{H_2}^{max}$ denote the imposed upper bounds on $LPSP_e$ and $LPSP_{H_2}$, respectively.

4.2.2. System-wide power balance

According to Eq. (42), at each time-step of the system operation, the sum of all of the internally generated energy components, energy releases from the storage media, energy imports from the main grid, and any unmet load must be equal to the sum of the total energy consumed within the MG (to serve the loads or to charge the energy storage devices) and any power sold to the upstream grid.

$$\begin{aligned}P_{PV}(t) + P_{WT}(t) + P_{MH}(t) + P_{BP}(t) + P_{dch}(t) + P_{FC}(t) + P_{im}(t) + P_{FCEV2G}(t)\\ + \frac{Q_L(t)}{\eta_I} + \frac{Q_{H_2}(t)}{\eta_S} = P_{ch}(t) + P_E(t) + P_{ex}(t) + \frac{P_L(t)}{\eta_I} + \frac{P_S(t)}{\eta_S} \forall t,\end{aligned} \tag{42}$$

where $Q_L(t)$ and $Q_{H_2}(t)$ respectively represent the unmet electrical and hydrogen demands at time-step t, which are used in the LPSP calculations.

4.2.3. Demand response scheduling

As mentioned previously, under equilibrium conditions of the proposed two-stage, aggregator-mediated, market-driven DR arrangement, the constraints in Eqs. (24), (25), (27), (28), (30), (31), (33) must be relaxed.

4.2.4. Energy storage systems and fuel cell electric vehicles

The optimisation of the MG equipment capacity must additionally adhere to some constraints in terms of charge/discharge rate limits of the energy storage media and FCEVs, bounding the state of charge/hydrogen of the storage systems and vehicles, as well as the state of energy reserves in the first and last operating hours, which could be expressed mathematically as:

$$E_{es,min} \le E_{es}(t) \le E_{es,max} \forall t, es, \tag{43}$$

$$P_{es}^{ch,min} \le P_{es}^{ch}(t) \le P_{es}^{ch,max} \forall t, es, \tag{44}$$

$$P_{es}^{dch,min} \le P_{es}^{dch}(t) \le P_{es}^{dch,max} \forall t, es, \tag{45}$$

$$E_{es-\{FCEV\}}(0) = 0.5 \times E_{es-\{FCEV\},max} \forall es, \tag{46}$$

$$E_{es-\{FCEV\}}(8760) \ge E_{es-\{FCEV\}}(0) \forall es, \tag{47}$$

where $E_{es}(t)$ is the energy content of the energy storage technology $es \in ES = \{B, SC, HT, FCEV\}$ at time-step t; $E_{es,min}$ and $E_{es,max}$ respectively denote the minimum and maximum allowable energy content of energy storage technology es; $P_{es}^{ch}(t)$ and $P_{es}^{dch}(t)$ respectively represent the

charging and discharging rates of storage technology *es* at time-step *t*; $P_{es}^{ch,max}$ and $P_{es}^{dch,max}$ are the maximum charging and discharging rates of storage technology *es*, respectively; and $P_{es}^{ch,min}$ and $P_{es}^{dch,min}$ are the minimum charging and discharging rates of storage technology *es*, respectively.

The maximum allowable energy content of the battery bank, SC bank, and hydrogen tank are defined by their optimised capacity at each iteration of the optimisation process, whereas the maximum total energy content of the releasable hydrogen stored in the FCEVs' tanks ($\max(P_{FCEV2G}^{max}(t)\Delta t)$ where $t \in T$) is limited by the maximum (optimal) capacity of the FCEV2G setup (as part of the hydrogen station) in addition to the stored hydrogen in the vehicles' tanks at time-step *t*. That is, the variables $E_{es,max}$, $es \in ES$ are treated as endogenous variables in the model. Also, the same principle holds for the variables $P_{es}^{ch,max}$ and $P_{es}^{dch,max}$.

Moreover, in the interest of preventing the performance degradation–and mitigating the energy losses–during the start-up and shut-down cycles of the electrolyser, fuel cell, and biopower plant, a specific constraint preserves the durability of their operation. To this end, when the electrolyser, fuel cell, and biopower plant are started up, they are constrained to continue to run for at least t_{up} time-steps–as a minimum up-time constraint–at operating points equal to, or greater than the initially adjusted operating points. Accordingly, the power output from the fuel cell and biopower plant are treated as negative loads in the course of the MG operation on the extra hours mentioned above, whilst also being allowed to take higher operating point values where appropriate.

In addition, to avoid severe pressure drops in the hydrogen tank, complete releases of hydrogen are prevented by enforcing $E_{HT,max}$ not to fall short of 5% of the optimised capacity of the tank. Also, to ensure that the design pressure of the tank is not exceeded, the upper limit on the energy content of the tank is set as 95% of its optimum capacity [107].

4.2.5. Energy exchange

The MG's transactions of energy with the upstream power network is constrained by Eqs. (9) and (10) to adhere to the optimal size of the transformer connecting the MG system with the upstream grid at the point of common coupling (PCC).

4.2.6. Decision variables

Specific upper bounds are set for maximum values the non-negative design variables can take, as represented in Eq. (48). These bounds are adjusted commensurate with the practical feasibility of implementing the conceptualised MG system in the considered area. For example, land limitations, characteristics of the catchment sites, available biomass as a feedstock, and acceptable emissions limits (from the biopower plant) could constrain the feasible solution space.

$$N_c \leq N_c^{max} \forall c, \tag{48}$$

where subscript $c \in C$ indicates the MG components, the optimal size of which is under investigation, while the superscript *max* denotes the maximum permissible value of the optimum quantity/capacity of the equipment (N_c).[6]

4.3. Meta-heuristic optimisation algorithm

Mathematically, the underlying MG capacity-planning model is a nonlinear, non-convex, non-deterministic polynomial time-hard (NP-hard) decision problem at its core, as indicated by Chen et al. [108]. Consequently, it cannot be solved exactly or by enumerating the entire search space explicitly or implicitly, but *meta*-heuristic techniques could be used effectively to solve the problem.

As noted earlier, the MFOA is employed to optimise a solution to the formulated MG capacity-optimisation problem on account of its well-proven superior performance to a wide range of both the well-established and state-of-the-art *meta*-heuristics in the MG planning context. Furthermore, owing to the mixed-discrete-continuous structure of the formulated problem, the technique proposed by Chowdhury et al. [109] is employed to modify the original continuous MFOA to make it applicable to the problem at hand. Moreover, the control parameters of the algorithm were adjusted as suggested by its developer [100], while the number of search agents, N_{SA}, and the maximum number of iterations, $Iter_{max}$, were set based on the findings of Khan and Singh [110] on the appropriate values to ensure the convergence of a broad spectrum of *meta*-heuristic optimisation algorithms–including both the well-established and state-of-the-art *meta*-heuristics–in the context of MG design optimisation and capacity planning.

4.4. Data: Adjusted demand-response integrated micro-grid equipment capacity planning model parameters

Table 4 lists the chosen data values for the parameters used to build the proposed DR-integrated MG equipment capacity-planning model.

4.5. Overview of the proposed solution algorithm

The flowchart of the proposed MG equipment capacity-planning model, which uses the proposed two-stage, aggregator-mediated market-driven DR model to realistically project the customer engagement in incentive-based DR programmes–based on an economically stable allocation of the profits generated from interruptible load programmes between the sole energy service provider, DSM aggregators, and end-users–is presented in Fig. 8. As can be seen from the figure, the solution algorithm integrates the proposed DR provision framework (the yellow block) and applies the developed rule-based hourly-basis operational scheduling strategy (the light coral block), while taking an iterative approach to optimise the discounted MG investment cost with which to determine the respective size of the equipment (the blue blocks).

Table 4
Data values for the demand response-integrated micro-grid equipment capacity planning model parameters.

Scalar	Value	Scalar	Value
$E_{es,max}$	(endogenous variable)	N_{FCEV2G}^{max}	5,000 kW
$E_{es-\{HT\},min}$	0 kWh*	N_{HT}^{max}	50,000 kg
$E_{HT,min}$	(endogenous variable)	N_{MH}^{max}	30
i_{MGO}	$0.02/kWh	N_{PV}^{max}	20,000
I_{MGO}^{min}	$0.02/kWh	N_{SA}	100
I_{MGO}^{max}	$0.32/kWh	N_{S}^{max}	100 kg-H_2/h
$I_{LA}^{j,min}$	$(0.02$−$\varepsilon^{\dagger})$/kWh	N_{SC}^{max}	10,000
$I_{LA}^{j,max}$	$(0.32$−$\varepsilon^{\dagger})$/kWh	N_{T}^{max}	8,000 kVA
$Iter_{max}$	500	N_{WT}^{max}	15
$LPSP_{e}^{max}$	0%	$P_{es}^{ch,max}$	(endogenous variable)
$LPSP_{H_2}^{max}$	5%	$P_{es}^{ch,min}$	$\varepsilon^{\dagger}$ kW
N_{B}^{max}	20,000 kWh	$P_{es}^{dch,max}$	(endogenous variable)
N_{BP}^{max}	50	$P_{es}^{dch,min}$	$\varepsilon^{\dagger}$ kW
N_{E}^{max}	1,000	pen_{const}	$(1/\varepsilon^{\dagger})$
N_{FC}^{max}	2,000	t_{up}	3 h

* Note that the depth of discharge capability of the vanadium redox flow battery is 100% and the total energy content of the FCEVs' tanks is assumed to be aware of the specific level of hydrogen expected (desired) by each FCEV owner at the scheduled departure time.

† The symbol ε denotes a small positive infinitesimal quantity.

[6] The maximum permissible values of the design variables are aware of the rated powers of the corresponding components.

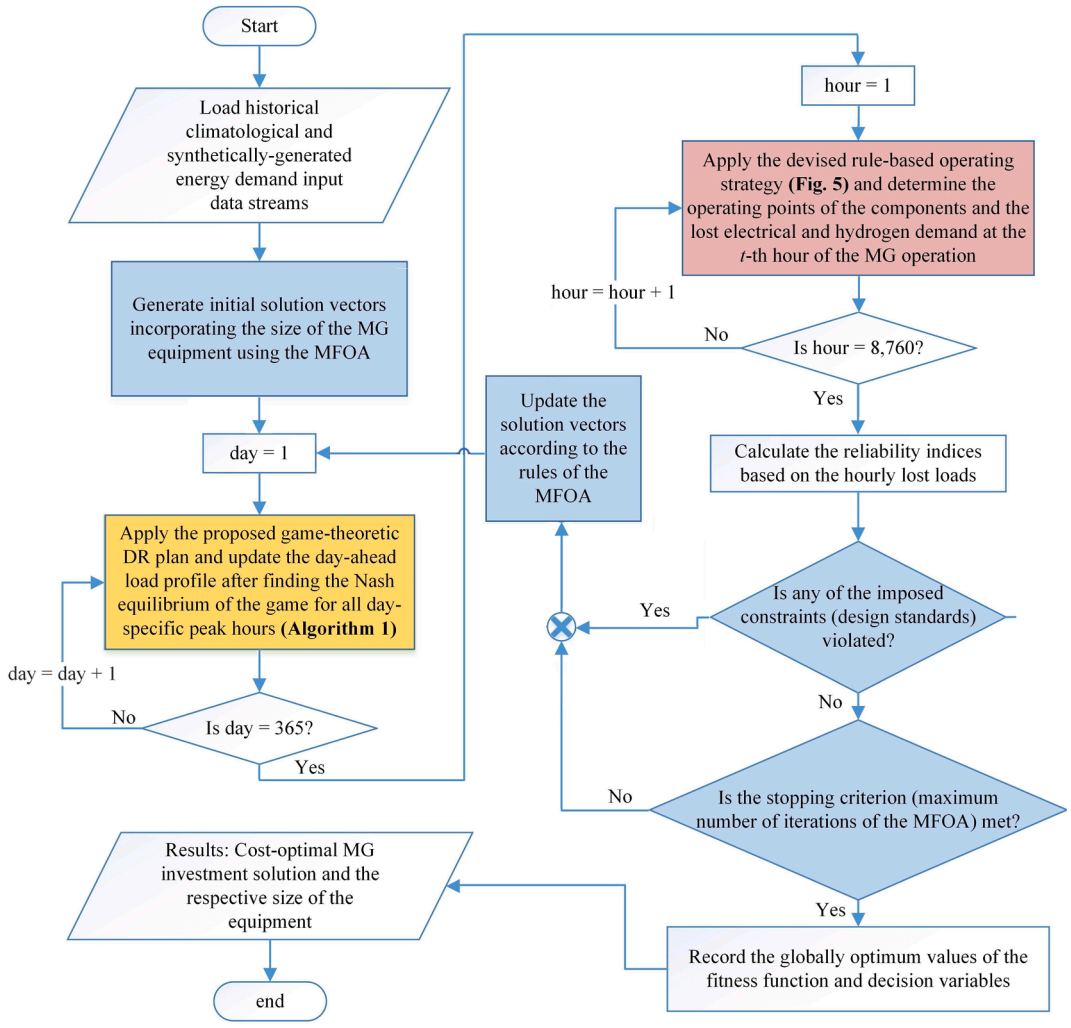

Fig. 8. Flowchart of the proposed non-cooperative game-theoretic DR-integrated approach for the optimal capacity planning of MGs.

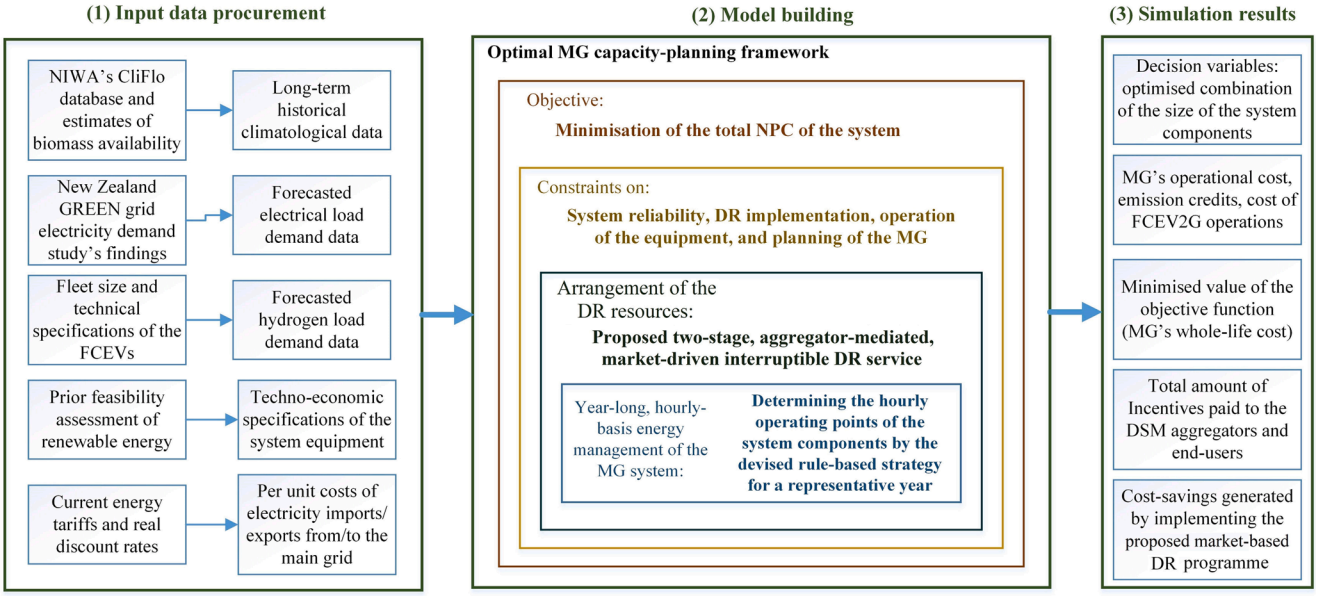

Fig. 9. Diagrammatic representation of the step-wise procedure for implementing the proposed optimal MG planning framework.

Furthermore, the step-wise representation of the integrated simulation platform to optimally design the conceptualised MG, while managing the DR resources using the proposed DR scheduling approach is summarised in Fig. 9. After the procurement and pre-processing of the input data, the model is built up in a multi-layered structure, which consists of (from bottom to top): (1) a rule-based hourly energy scheduling strategy, (2) a two-stage, aggregator-mediated, DSM market design to arrange the delivery of the DR resources on a day-ahead basis, (3) various constraints the objective function is subjected to, and (4) the derived fitness function representing the whole-life cost of the system, which is to be optimised using the MFOA.

5. Case study

To confirm the proposition put forward in Section 1 on the effectiveness of integrating the proposed DR management framework into the standard *meta*-heuristic-based MG capacity planning approach, as well as the viability of the conceptual test-case MG system, laid out in Section 2, this section presents the results of the case study analysis conducted for the town of Ohakune, New Zealand. To this end, first, the validity of the model is confirmed through a direct comparison of the extreme-case model results with those of a business-as-usual (BAU), non-game-theoretic interruptible DR scheduling framework. Then, the economic viability of integrating the developed DSM strategies into the long-term MG investment decision-making processes is benchmarked against two cases where: (1) the DSM market is cleared without employing ideas from non-cooperative game theory for interactive decision-making regarding the practical capacity of DR resources, and (2) no provision is made to employ the responsive loads as a backup resource in the proposed MG system. Finally, a financial appraisal assessment demonstrates the economic sustainability of the proposed renewable energy project. Numerical simulations were carried out using the MATLAB software (version 9.5, R2018b) [111].

5.1. Case study site: The town of Ohakune, New Zealand

The notional MG system proposed in this study is envisioned to decarbonise the energy economy of the town of Ohakune, which is situated in the central part of the North Island of New Zealand–latitude 39.4180°S, longitude 175.3985°E [112].

The forecasted hourly-basis, year-long climatic input data streams, are presented as monthly mean 24-h profiles in 3D plots in Fig. 10 [76]. Also, the forecasted monthly averaged profile for biomass availability is shown in Fig. 11, assuming that the amount of monthly available biomass is evenly distributed over the days of the months [113,114].

The forecasted one-year load power demand on the system, which is represented as a monthly mean 24-h profile for greater clarity, is shown in a 3D plot in Fig. 12 (a) [115,116]. Also, the forecasted monthly mean

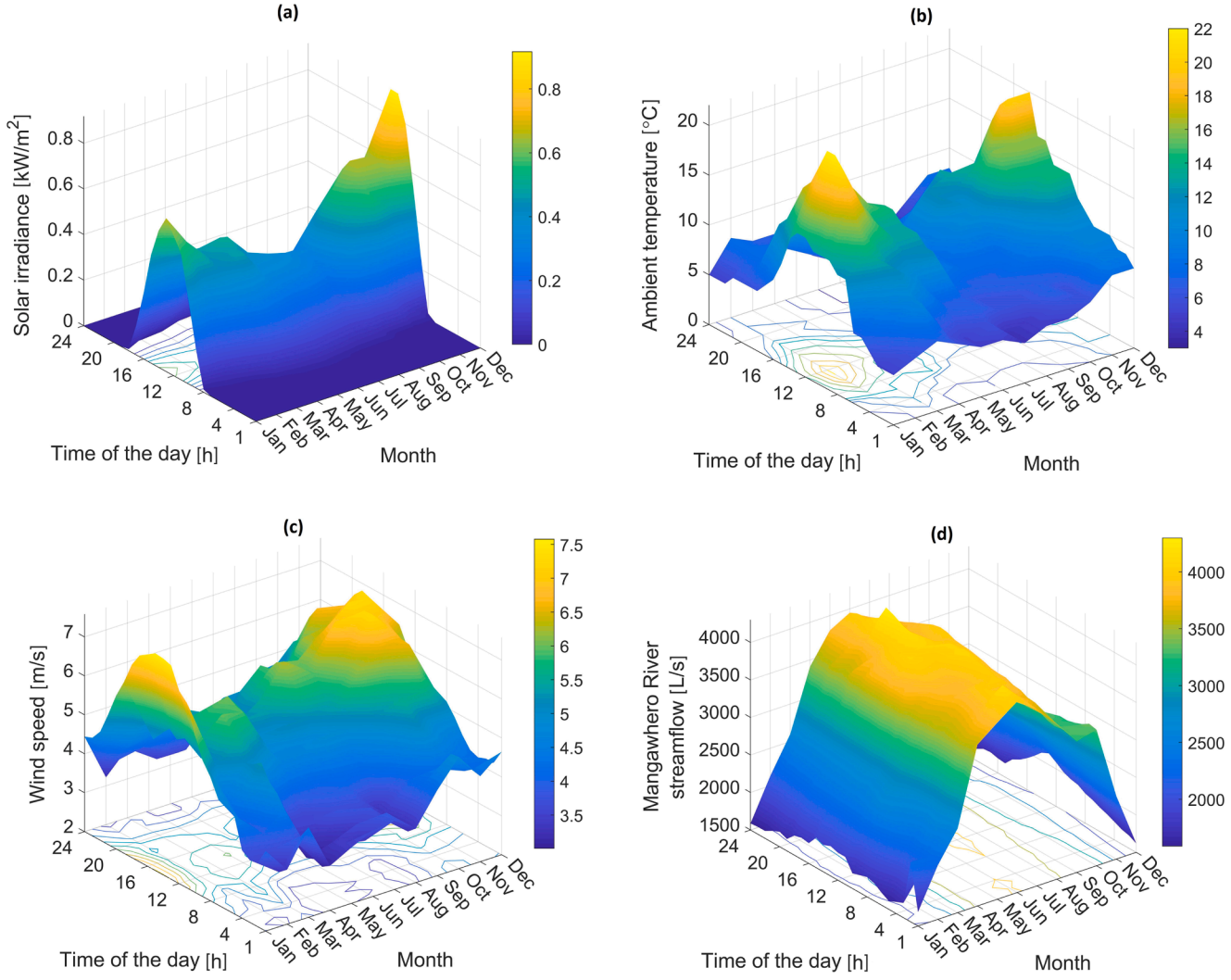

Fig. 10. CliFlo-compliant forecasted meteorological input data (at an hourly resolution) for Ohakune, New Zealand: (a) solar irradiance; (b) ambient temperature; (c) wind speed; and (d) streamflow.

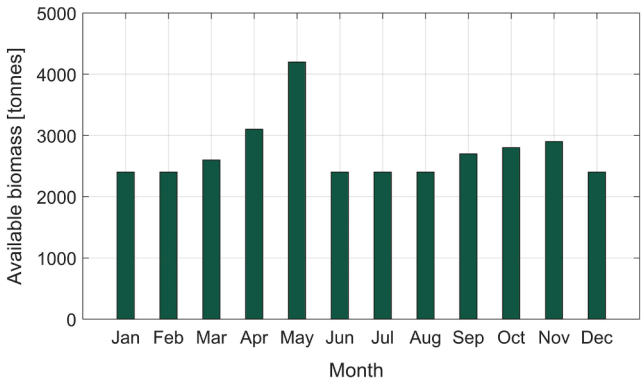

Fig. 11. Monthly mean profile for the estimated total biomass available per month at the site: Ohakune, New Zealand.

24-h profile for the hydrogen demand of the refuelling station–considering the seasonal variation in demands for transportation fuel as suggested in [117]–is shown in a 3D plot in Fig. 12 (b).

The forecasted hourly-basis, year-long wholesale electricity price input data stream, $\pi_{im}(t)$, obtained using the weighted rolling average method, is shown as a monthly averaged daily profile in Fig. 13 [118].

More details of the case study site and the complete details on how the forecasted one-year profiles for climatological, load demand, and wholesale electricity price data are derived, can be found in Supplementary Material (Additional File 3: Case study details).

Table 5 presents the data values and sources for all parameters of the proposed two-stage, aggregator-mediated, incentive-based DSM framework. In addition to the values of the model parameters defined in Section 3, Table 5 presents the number of customers signed up with each aggregator, which is denoted by N^{j}_{cust}.

Moreover, given the New Zealand government's aspirations of electrifying transport to help meet its target of net-zero greenhouse gas emissions by 2050, as well as the recent government-funded 'Warmer Kiwi Homes' programme offering up to 90% heat pump grants to low-income home owners, the penetration levels of light-duty FCEVs and heat pumps were assumed to be 40% and 60%, respectively at the time of commitment. Accordingly, smart charging of FCEVs and control of heat pump demand is of utmost importance to smooth and manage the overall load during peak periods.

5.2. Validation of the proposed demand-side management market

To validate the effectiveness of the proposed two-stage aggregator-mediated DSM market model, two instances of day-ahead energy management analysis are conducted and the obtained results are compared with the case where the aggregator-mediated interruptible/curtailable DR resources are scheduled in a BAU way. Accordingly, the non-market-driven (BAU) procurement of aggregator-activated interruptible/curtailable responsive loads excludes the ability to adaptively update the incentives offered by the MG operator, based on which the aggregators post their incentives to the retail DSM market, and subsequently the end-consumers select their participation rate in load reduction programmes. More specifically, the MG operator offers a fixed, day-specific rate of incentive to the aggregators, who also offer fixed levels of incentives to their customers–for load reduction during the peak hours of electricity consumption. Subsequently, the end-users and aggregators respond to the aggregator-determined and MG operator-offered incentive rates, respectively. In this way, the retail and wholesale DSM markets are sequentially cleared for the day-specific incentives by stacking the customers' and aggregators' bids, low to high, and allocating demand reduction schedules to the customers and aggregators in the merit order irrespective of whether the power shortage is addressed with the best compromise between load reduction and imported electricity for each hourly period. Expectedly, as there exists no mechanism to update the

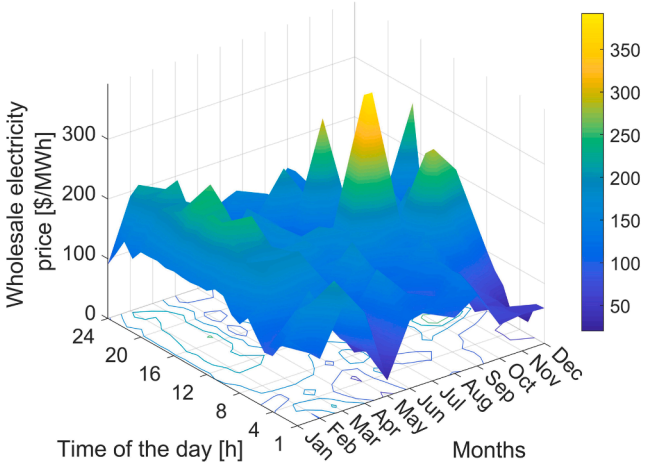

Fig. 13. Forecasted monthly mean 24-h profile for the wholesale power price.

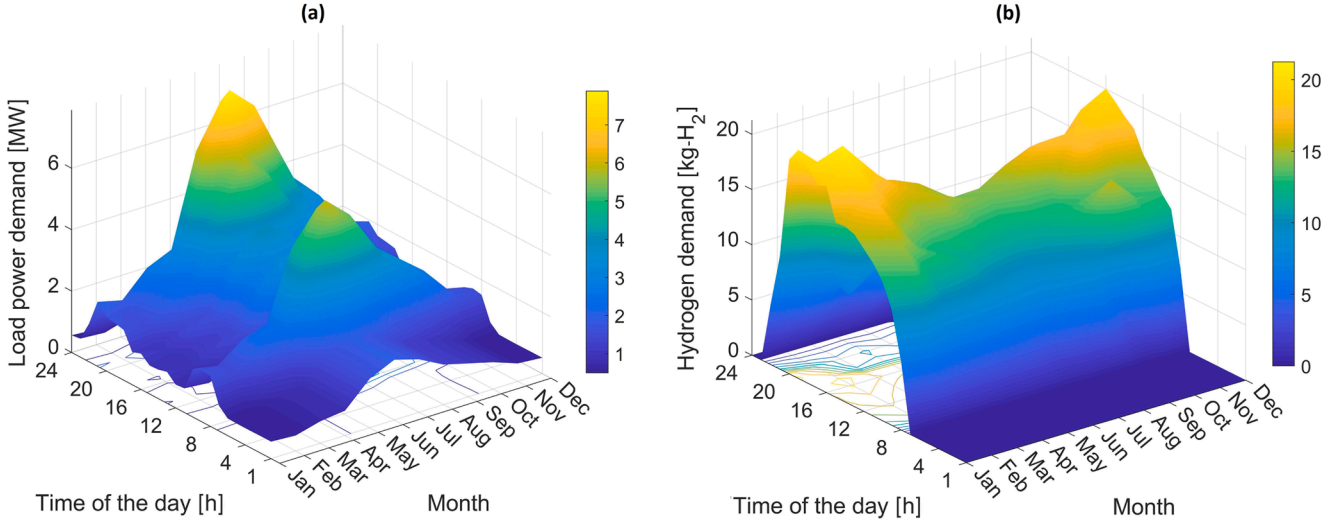

Fig. 12. Forecasted monthly mean 24-h profiles for the energy demand of the town Ohakune: (a) load power demand; and (b) hydrogen demand.

Table 5
Data values and assumption sources for the two-stage, aggregator-mediated, incentive-based demand-side management framework.

Parameter		Aggregator				
		Residential	Commercial	Industrial	Agricultural	FCEV-refuelling
δ_j*	Value	0.48	0.51	0.57	0.63	0.76
	Source	[119]	[119]	[119]	[119]	[120]
$c_1^{k,j}$ [$/kWh^2]	Range	[1.08×10^{-3}, 1.15×10^{-3}]	[1.04×10^{-3}, 1.07×10^{-3}]	[0.99×10^{-3}, 1.03×10^{-3}]	[0.95×10^{-3}, 0.98×10^{-3}]	[0.91×10^{-3}, 0.94×10^{-3}]
	Source†	[121,122]	[121,122]	[121,122]	[121,122]	[121,122]
$c_2^{k,j}$ [$/kWh]	Range	[11.49×10^{-3}, 11.70×10^{-3}]	[11.31×10^{-3}, 11.48×10^{-3}]	[11.71×10^{-3}, 11.86×10^{-3}]	[11.25×10^{-3}, 11.30×10^{-3}]	[11.40×10^{-3}, 11.57×10^{-3}]
	Source†	[121,122]	[121,122]	[121,122]	[121,122]	[121,122]
$d_{full}^{k,j}$ [kWh]	Range	[8, 30]	[20, 100]	[100, 200]	[30, 65]	[5, 30]
	Source	(this paper)	(this paper)	(this paper)	(this paper)	(this paper)
$d_{ncr}^{k,j}$ [kWh]	Range	[2.5, 16.5]	[5, 60]	[20, 84]	[10, 46.2]	[4, 25.5]
	Source	(this paper)	(this paper)	(this paper)	(this paper)	(this paper)
N_{cust}^{j}	Value(s)	250	65	10	55	{1, 2, …, 150}‡
	Source	(this paper)	(this paper)	(this paper)	(this paper)	(this paper)

* The load type-dependent DR procurement factor (sectoral elasticity of customer-supplied DR capacity) for the residential, commercial, industrial, and agricultural loads (normalised to the range [0, 1]) were adjusted in proportion with the weighted average values of unserved energy for various durations of interruption in a New Zealand context [119], while this factor for the FCEV-refuelling load was adjusted based on the plug-in EVs' value of lost load reported in [120].

† The range of values the discomfort tolerance coefficients of customers can take were arbitrarily selected. The chosen values were guided by those used in [121,122] for the customer outage cost function coefficients for the relevant customer categories. Additionally, the range of sector-wide customer discomfort tolerance coefficients was normalised with respect to the corresponding load type-dependent DR procurement factor (in an inversely proportional manner).

‡ Since the number of FCEVs that utilise the filling station's equipment varies with the time of day, it was modelled as a range of possible scenarios, i.e. the number of vehicles.

Table 6
Comparative analysis of the proposed and BAU realisations of the interruptible DR programme on the extreme days: February 14th and July 21st.

MG operator-offered incentive* (I_{MGO}) [$/kWh]		Total daily incentive payment to the aggregators ($I_{MGO}^{p}(\sum_{p\in P_d}\sum_{j\in J}D_{LA}^{j,p})$) [$/d]		Total daily incentive payment to the customers ($\sum_{p\in P_d}\sum_{j\in J}I_{LA}^{j,p}D_{LA}^{j,p}$) [$/d]		Total daily load reduction procured by the customers ($\sum_{p\in P_d}\sum_{j\in J}\sum_{k\in N_j}d^{k,j,p}$) [kWh/d]		Total daily cost of electricity imports ($\sum_{p\in P_d}cost_{im}^{p}$) [$/d]		Total daily operational cost of the MG ($\sum_{p\in P_d}OC_{MG}^{p}\sum_{p\in P_d}OC_{MG}^{p}$) [$/d]	
Feb. 14th	Jul. 21st	Feb. 14th	Jul. 21st	Feb. 14th	Jul. 21st	Feb. 14th	Jul. 21st	Feb. 14th	Jul. 21st	Feb. 14th	Jul. 21st
Business-as-usual interruptible DR scheduling approach											
0.02	0.02	10.5	43.3	3.9	15.6	525.0	2165.0	870.8	1997.7	881.3	2041.0
0.04	0.04	22.5	102.1	9.2	41.9	562.5	2552.5	863.2	1916.1	885.7	2018.2
0.06	0.06	44.8	162.8	18.8	70.0	746.7	2713.3	824.3	1882.4	869.1	2045.2
0.08	0.08	81.7	390.4	35.9	171.8	1021.3	4880.0	766.6	1427.4	848.3	**1817.8**
0.1	0.1	180.9	528.5	83.2	232.5	1809.0	5285.0	601.2	1342.3	**782.1**	1870.8
0.12	0.12	217.1	634.2	91.8	310.8	1809.0	5285.0	601.2	1342.3	818.3	1976.5
0.14	0.14	264.7	787.8	105.9	409.7	1890.7	5627.1	584.1	1270.5	848.8	2058.3
0.16	0.16	302.5	900.3	115.8	459.2	1890.7	5627.1	584.1	1270.5	886.6	2170.8
0.18	0.18	377.3	1013.7	188.7	547.4	2096.1	5631.7	540.9	1269.5	918.2	2283.2
0.2	0.2	421.5	1341.0	219.2	643.7	2107.5	6705.0	538.5	1044.1	960.0	2385.1
0.22	0.22	486.0	1611.0	233.3	757.2	2209.1	7322.7	517.3	914.4	1003.3	2525.4
0.24	0.24	551.8	2093.1	253.8	879.1	2299.2	8721.3	498.3	620.7	1050.1	2713.8
0.26	0.26	708.6	2593.3	311.8	959.5	2725.4	9974.2	408.9	357.6	1117.5	2950.9
0.28	0.28	1040.2	2906.8	436.9	1133.6	3714.9	10381.4	201.2	272.1	1241.4	3178.9
0.3	0.3	1401.8	3503.2	560.7	1191.1	4672.7	11677.3	0	0	1401.8	3503.2
0.32	0.32	1495.2	3736.7	586.2	1195.7	4672.7	11677.3	0	0	1495.2	3736.7
Proposed market-driven interruptible DR scheduling approach											
0.17	0.15	566.3	1327.8	230.7	488.6	3253.8	8155.2	50.8	76.9	617.1	1404.7

Values in bold indicate the total daily operational cost of the MG in the best performance of the BAU interruptible DR management framework.

* Given the variability of the best-strategy incentive offered by the MG operator at different peak hours of the day in the proposed market-driven model, the mean daily value of the optimal incentive rate offered by the MG operator ($\overline{I_{MGO}^{p,*}}$) is presented for the proposed model.

initial strategy of the MG operator, the efficiency of such a framework is particularly sensitive to the choice of the MG operator-offered incentive rate. Hence, the model response is determined for various day-specific MG operator-offered incentive rates. Accordingly, Table 6 summarises the results obtained by simulating the above-described BAU interruptible DR mechanism when applied to the DR provision problem at hand in two extreme scenarios with the MG operator-offered incentive payment ranging from $0.02/kWh to $0.32/kWh in intervals of $0.02/kWh. Specifically, the two days that represent the most intense peak and trough on the year-round, mean daily load profile (consisting of the mean of the load power demand forecasts for 24 equidistant times in the course of each continuous 24-hour period of the representative year), namely July 21st and February 14th, were chosen for scenario analysis. The table, furthermore, presents the results of the suggested market-driven interruptible DR model for the extreme days considered.

The following observations can be made from a comparative analysis of the proposed model and BAU model results presented in Table 6:

1. The systematic updating of the MG operator-offered incentive for load reduction–for the time-steps at which the system is predicted to be under stress–using an aggregator-mediated, market-driven DSM market model, can play a pivotal role in unlocking the full potential of demand-side resources by finding the economically efficient DR allocation solutions. In other words, the lack of a systematic

framework to enable the DR programme administrator to vary the rate of incentive payment to increase or decrease the supply of DR capacity, either results in an overpayment for access to the DR resources, or leads to the under-trading of the responsive loads. More specifically, the proposed model has outperformed the BAU model by at least ~21.1% (equating to a saving of $165) and ~22.7% (equating to a saving of $413.1) in terms of the daily operational cost of the MG ($\sum_{p\in P_d} OC^p_{MG}$) respectively for the February 14th and July 21st scenarios.

2. The BAU realisation of the interruptible DR programme has failed to exploit the full potential of the demand-side flexibility resources available. The most crucial factor underpinning this under-utilisation of the responsive loads in this model is the lack of interaction between the MG operator and responsive load aggregators, as well as between aggregators and end-consumers to dynamically re-render the incentives for load reduction at different times of the day. This is evident from Table 6, where increasing the MG operator-posted incentive rate from $0.1/kWh to $0.12/kWh, and also from $0.14/kWh to $0.16/kWh, has only led to an increase in the total daily payment to the aggregators despite no increase in the net load reduction in both the scenarios considered.
3. In contrast to the proposed model where the daily operational cost of the system strictly decreases as the MG operator-offered incentive rate increases up to a saturation point, the BAU model's response to variations in the MG operator-offered incentive rate does not tend to follow a particular pattern. For example, increasing the MG operator-offered incentive rate from $0.02/kWh to $0.04/kWh in the case of July 21st has resulted in a reduction of the daily operational cost of the MG by ~1.1%, then increasing the incentive rate from $0.04/kWh to $0.06/kWh has increased the daily operational cost of the MG by ~1.3%, and then increasing the incentive rate from $0.06/kWh to $0.08/kWh has substantially driven down the daily operational cost of the MG system–to the globally optimal level. Much of the reason for such an erratic behaviour of the BAU model lies in the fact that the participation of the aggregators depends on meeting certain threshold levels of profits. Put differently, increasing the rate of incentive payments leads to a worthless overpayment unless it triggers the participation of a further MG customer, provided that a lower incentive rate than the per-unit cost of electricity import is deemed sufficient by the customer. However, the interactive DSM market-clearing mechanism embedded in the proposed DSM market model–implemented using the proposed interactive value iteration solution approach (refer to Algorithm 1)–has addressed such a source of unreliability.

To evaluate the weather-sensitivity of each model, the analysis is expanded to include all the days in which the interruptible DR programme is executed. Table 7 summarises the descriptive statistics for the DR scheduling variables during the hours of peak demand for which a net energy deficit is predicted. Note the change in temporal resolutions of the dependent variables compared to Table 6. Specifically, the results are presented for the morning peak (MP) and evening peak (EP) hours across the seasons to provide insight into the temporal distribution of utilising the DR resources.

The table is revealing in the following ways:

1. The DR events occur more frequently in autumn (734 times) and winter (832 times) than in spring (388 times) and summer (284 times). A comparison of the total number of DR event observations during the morning and evening peak periods across different seasons offers the following insights: (i) two distinctive daily periods of positive net load demand–the total electric demand on the system minus local generation–can be identified for autumn and winter; while (ii) the net load demand in spring and summer is characterised by one period, namely the MP. This change in the capacity deficit pattern is mainly driven by weather conditions; the warmer months reduce the necessity of utilising electric space heating systems. Other seasonal covariates, including daylight saving and longer daylight hours in spring and summer, which lead to both lower lighting use and higher solar PV generation in the early evening, also contribute to this variation, albeit to a lesser degree.
2. Although the number of DR events that occurred during the MP period is lower than the corresponding EP period in the colder months, the average hourly load reduction procured is nearly the same for the morning and evening peak periods in autumn and winter. This implies that the profile of the net load demand has a shorter, sharper peak in the morning, but a longer, flatter peak in the evening in autumn and winter. This is not only due to the

Table 7
Summary statistics for the DR scheduling variables.

Variable		Spring		Summer		Autumn		Winter	
		MP	EP	MP	EP	MP	EP	MP	EP
MG operator-offered incentive [$/kWh]	Avg.	0.159	0.202	0.140	0.168	0.120	0.097	0.128	0.183
	Med.	0.160	0.200	0.140	0.173	0.120	0.097	0.120	0.189
	SD	0.031	0.034	0.026	0.027	0.015	0.038	0.039	0.029
	Obs.	291	97	208	76	344	390	400	432
Incentive payment to the aggregators [$/h]	Avg.	49.004	111.484	26.866	62.378	48.504	63.166	77.043	147.260
	Med.	47.409	101.634	26.492	61.087	48.996	64.636	78.349	147.850
	SD	11.852	26.799	4.103	5.268	1.665	5.667	6.336	8.320
	Obs.	291	97	208	76	344	390	400	432
Incentive payment to the customers [$/h]	Avg.	20.092	51.281	12.105	29.448	22.627	28.039	30.510	67.382
	Med.	20.115	52.360	10.606	29.282	20.901	27.432	29.660	67.446
	SD	5.570	5.954	6.314	2.940	6.307	3.483	4.240	4.252
	Obs.	291	97	208	76	344	390	400	432
Load reduction procured by the customers [kWh]	Avg.	308.201	551.901	191.900	371.298	604.200	651.196	801.898	804.699
	Med.	311.051	553.074	192.312	371.649	603.094	651.628	804.004	805.741
	SD	9.814	11.053	5.593	11.579	6.587	11.687	9.678	6.922
	Obs.	291	97	208	76	344	390	400	432
Cost of electricity imports [$/h]	Avg.	8.611	15.237	3.985	7.907	5.531	8.402	9.004	17.516
	Med.	9.044	15.780	4.238	7.974	5.406	7.941	8.172	17.049
	SD	3.531	2.020	0.881	0.187	1.087	1.873	2.556	4.937
	Obs.	291	97	208	76	344	390	400	432
Total operational cost of the MG [$/h]	Avg.	57.615	126.721	30.851	70.285	54.035	71.568	86.047	164.776
	Med.	56.453	117.414	30.730	69.061	54.402	72.577	86.521	164.899
	SD	2.618	7.981	2.771	3.217	2.410	3.651	4.206	9.325
	Obs.	291	97	208	76	344	390	400	432

coincidence of the residential load with the start of the business day, but also the fact that non-dispatchable renewable power generation from wind and hydro resources is considerably less during the autumn and winter MP period than the corresponding EP period (see Fig. 10). Crucially, the proposed non-cooperative game-theoretic DR scheduling model has yielded reductions in load demand of, on average, ~24% and ~22% respectively during the winter morning and evening peak periods. This equates to an average hourly energy reduction of ~802 kWh in the MP and ~805 kWh in the EP. In summer, this percentage decreases to ~13% (192 kWh) in the MP, and ~15% (371 kWh) in the EP period.

3. Defining the data skewness as (mean–median) / standard deviation, it can be shown that the skewness values of the 'cost of electricity imports' and the 'incentive payments made by the utility to the aggregators' datasets have opposite signs at all the eight quarterly time intervals. For example, the skewness values of the above-mentioned datasets for the winter MP period are 0.326 and −0.206, respectively. Accordingly, the mean of the former dataset is greater than its median (i.e., the dataset distribution is positively skewed), whereas the mean of the latter dataset is less than its median (i.e., negatively skewed). This suggests that the optimal trade-off between imported power and utilised DR capacity tends to follow an approximately consistent pattern during each period of peak electricity use. This finding corroborates the robustness and validity of the proposed non-cooperative game-theoretic DSM approach in producing the best compromise between the imported power and elicited DR capacity.

Moreover, Table 8 provides a statistical evaluation of the efficacy of the proposed market-based integration (MBI) of responsive loads using non-cooperative game theory as compared to the BAU model in the four seasons. Note that, for reasons of space, the modelling results are not broken down into the morning and evening peak periods.

From Table 8, emerge a number of key statistically valid evidence to support the superiority of the proposed game-theoretic DR scheduling model to the BAU interruptible programmes:

1. The proposed aggregator-mediated, market-based DR programme is able to unlock new sources of economic value that are inaccessible by the BAU-DR scheduling approach. This has resulted in a ~17% (equating to ~$39 k) reduction in the operational cost of the MG in the baseline year. In large part, this is because the proposed model ensures a level playing field for all the DR providers and equitably allocates the benefits of third-party DR aggregation, whilst additionally providing a platform for the MG operator, DRAs, and end-consumers to mutually optimise their portfolios and determine the lowest operational costs.
2. A comparison of the seasonal performance of the proposed model and the BAU approach reveals that, on average, the DR resources are under-utilised in autumn and winter, whilst additionally the DR providers are over-compensated in spring and summer in the BAU approach. More specifically, in contrary to the obtained results from the proposed model, where the distributions of the 'incentive payments to the aggregators' and the 'cost of electricity imports' data are oppositely skewed, they have similar skewness patterns in the BAU approach. The BAU approach's results indicate that both of the above-mentioned distributions are skewed to the left (i.e., most of the observations lie to the right of the mean) in spring and summer, whereas they are both positively-skewed (i.e., most of the observations lie to the left of the mean) in autumn and winter. A major explanation for this is the BAU interruptible service approach's incapability to provide a more-targeted, non-prespecified incentive price signal that fluctuates hourly reflecting changes in the wholesale prices of electricity.
3. While the percentage of incentive payments to the customers to the incentive prices received by the aggregators remains nearly the same across the seasons in the proposed game-theoretic modelling results (within the range of approximately 43–46%), the percentage varies significantly from season to season if the problem is solved in a BAU way. In particular, the BAU modelling results yield the highest utility margin for the customers (with the customers' share of the utility incentives of ~53%) during the winter months (June to August) when their use of electricity for heating contributes to high network loads. On the other hand, the per-unit profit of the DRAs is largest during the summer months (December to February) when electric

Table 8
Comparative statistical analysis of the proposed and BAU-DR scheduling models.

Variable		Spring		Summer		Autumn		Winter	
		BAU*	MBI	BAU*	MBI	BAU*	MBI	BAU*	MBI
MG operator-offered incentive [$/kWh]	Avg.	0.147	0.170	0.112	0.148	0.051	0.109	0.073	0.155
	Med.	0.152	0.159	0.108	0.146	0.045	0.110	0.074	0.156
	SD	0.017	0.033	0.017	0.029	0.025	0.031	0.030	0.028
	Obs.	388	388	284	284	734	734	832	832
Incentive payment to the aggregators [$/h]	Avg.	16.821	64.624	9.725	36.369	13.342	55.595	35.537	111.054
	Med.	16.874	55.729	9.777	29.113	12.242	51.287	33.964	87.232
	SD	1.670	31.920	0.863	5.482	4.387	8.279	5.125	35.922
	Obs.	388	388	284	284	734	734	832	832
Incentive payment to the customers [$/h]	Avg.	6.390	27.889	3.112	16.746	6.538	25.245	18.835	48.370
	Med.	6.454	23.463	3.223	13.639	6.458	25.131	17.657	36.607
	SD	0.574	14.624	0.279	9.624	1.837	5.914	10.386	18.948
	Obs.	388	388	284	284	734	734	832	832
Load reduction procured by the customers [kWh]	Avg.	104.263	369.126	80.929	239.908	240.608	629.171	465.260	803.352
	Med.	104.979	314.339	81.951	194.866	238.388	512.418	463.248	714.444
	SD	7.450	106.143	4.920	79.940	14.018	123.846	16.353	101.754
	Obs.	388	388	284	284	734	734	832	832
Cost of electricity imports [$/h]	Avg.	76.462	10.268	41.742	5.034	61.044	6.919	113.148	13.127
	Med.	76.845	10.633	42.059	5.074	31.421	6.948	55.583	13.392
	SD	1.902	4.274	2.314	0.148	6.255	2.935	5.206	3.129
	Obs.	388	388	284	284	734	734	832	832
Total operational cost of the MG [$/h]	Avg.	93.283	74.892	51.467	41.404	74.386	62.515	148.685	124.181
	Med.	93.836	58.145	52.657	33.028	72.784	57.739	146.465	94.166
	SD	1.766	30.248	3.311	17.753	7.011	9.224	7.104	40.021
	Obs.	388	388	284	284	734	734	832	832

* The BAU results represent the business-as-usual model's best performance out of different daily utility-offered incentives ranging from $0.02/kWh to $0.32/kWh in intervals of $0.02/kWh.

heating cannot provide DR, which reduces the customers' share of revenues to as low as ~32%. This indicates the BAU approach's failure to provide a fair division of the utility-offered financial incentives between the DRAs and their corresponding customers, which results in the overall DR underperformance.

As these observations are shown to remain valid for the year-round operation of the system, their positive impact on the lifetime cost and cost-effectiveness of the conceptualised system is discussed in the next sub-section.

5.3. Optimal equipment capacity-planning results

To evaluate the effectiveness of the proposed DR scheduling framework in reducing the whole-life cost of MGs, the equipment capacity-planning of the conceptualised MG was carried out under three cases: (1) taking a BAU (static) interruptible load approach to managing the smaller DR resources (as detailed in Section 5.2), (2) using the proposed market-based (dynamic) integration of the aggregator-mediated interruptible responsive loads (presented in Section 3), and (3) not implementing any DSM strategies. Tables 9 and 10 present the MG investment planning model results under the above-mentioned three cases, which are respectively denoted by 'BAU-DR', 'MBI-DR', and 'NO-DR'. Specifically, Table 9 details a breakdown of the optimised cost components included in the life-cycle analysis of the MG system (see Eq. (39)), while Table 10 provides the optimum size of the MG equipment, which are the main decision variables of the optimisation problem. Note that the optimisation model results are adjusted for the value of biomass feedstock. To this end, the total cost associated with the pelletisation of blended biomass feedstocks–agricultural and woody biomass–was considered to be $72/tonne of pellets [123]. The case study site's natural endowment of forest biomass together with its temperate climate that is ideally suited to the agricultural activities, narrows, to a considerable extent, the feedstock supply uncertainty bounds. This provides strong support for taking an exogenous approach to account for the biomass feedstock costs–in the post-optimisation phase.

It is also noteworthy that the results reported in the tables represent the best-case performance of the MFOA out of 30 independent trials. Moreover, to demonstrate the adequacy of the maximum number of iterations, and the number of search agents considered, the convergence curves of the MFOA in its best and worst overall performances for each of the above-mentioned cases are shown in Fig. 14.

The comparative results presented in Table 9 reveal that the proposed market-based modelling of the interruptible DSM processes in the planning phase of the conceptualised MG reduces the estimated whole-life cost of the system by at least 21% and up to a maximum of 32% (with an incentive resolution of $0.02/kWh), as compared to the BAU interruptible DR-integrated and non-DR-integrated MG planning cases, respectively.

Table 10
Size of the MG equipment in the cost-minimal solution under different DR provision strategies.

Component		Simulation case		
		MBI-DR	BAU-DR	NO-DR
PV plant	N_{PV} [no.]	3,594	3,690	4,742
	STDEC* [%]	3.54	3.04	3.33
Wind plant	N_{WT} [no.]	4	5	6
	STDEC* [%]	24.11	26.35	26.73
Micro-hydro power plant	N_{MH} [no.]	6	6	6
	STDEC* [%]	1.91	1.59	1.36
Biopower plant	N_{BP} [no.]	4	4	7
	STDEC* [%]	0.77	0.64	0.96
Transformer	N_T [kVA]	310	320	329
	STDEC* [%]	0.11	0.10	0.08
Hydrogen tank	N_{HT} [kg]	6,079	7,904	9,168
	STDEC* [%]	16.93	18.11	18.16
Electrolyser	N_E [no.]	122	144	157
	STDEC* [%]	4.14	4.08	3.80
Fuel cell	N_{FC} [no.]	238	378	440
	STDEC* [%]	6.75	8.58	8.66
Battery bank	N_{1600} [no.]	2	2	2
	N_{400} [no.]	0	1	2
	N_{100} [no.]	2	0	3
	STDEC* [%]	17.49	15.06	16.00
Super-capacitor bank	N_{SC} [no.]	1,982	2,090	2,136
	STDEC* [%]	14.53	12.61	11.01
FCEV2G setup	N_{FCEV2G} [kW]	504	573	608
	STDEC* [%]	0.57	0.53	0.49
Hydrogen station	N_S [kg-H_2/h]	6.14	7.94	9.15
	STDEC* [%]	0.42	0.45	0.45
Inverter	N_{900} [no.]	5	6	7
	N_{115} [no.]	2	3	5
	N_{33} [no.]	1	3	1
	STDEC* [%]	8.73	8.86	8.97

* STDEC stands for the share of the total discounted equipment-related costs, which can be expressed explicitly in mathematical terms as $((\sum_{c\in C}\underset{20-yr}{NPC_c}) + \underset{20-yr}{NPC_I})$.

Table 9
Breakdown of the total discounted system cost under different DR provision strategies.

Cost component	Cost subcomponent	Simulation case		
		MBI-DR	BAU-DR	NO-DR
Total discounted equipment-related costs $((\sum_{c\in C}\underset{20-yr}{NPC_c}) + \underset{20-yr}{NPC_I})$ [$]		18.25 m	21.88 m	25.62 m
Total discounted MG operational costs $(\underset{20-yr}{NPV}(\sum_{t=1}^{8760} OC_{MG}(t)))$	Total discounted incentive payment to the aggregators $(\underset{20-yr}{NPV}(\sum_{t=1}^{8760} I_{MGO}(t)\sum_{j\in J} D^j_{LA}(t)))$ [$]	3.99 m	3.48 m	–
	Total discounted cost of electricity imports $(\underset{20-yr}{NPV}(\sum_{t=1}^{8760} cost_{im}(t)))$ [$]	0.46 m	2.76 m	7.46 m
Total discounted FCEV2G electricity provision costs $(\underset{20-yr}{NPV}(\sum_{t=1}^{8760} \pi_{FCEV2G} P_{FCEV2G}(t)))$ [$]		0.42 m	0.49 m	0.50 m
Total discounted operating costs of the biopower plant	Total discounted emission credits $(\underset{20-yr}{NPV}(\sum_{t=1}^{8760} cost_{em}(t)))$ [$]	0.52 m	0.57 m	0.62 m
	Total discounted biomass feedstock costs* $(\underset{20-yr}{NPV}(72 \times \sum_{t=1}^{8760} M_{BP}(t)))$ [$]	0.49 m	0.54 m	0.58 m
Total discounted income derived from electricity exports $(-\underset{20-yr}{NPV}(\sum_{t=1}^{8760} income_{ex}(t)))$ [$]		−2.41 m	−2.42 m	−2.97 m
Whole-life cost of the system (*WLC*) [$]		21.72 m	27.3 m	31.81 m

* The total cost of the biomass feedstock is not systematically affected by changes in the endogenous variables of the model in this study. That is, the total cost imposed by the biomass feedstock was calculated outside the optimisation model and the results were then corrected accordingly.

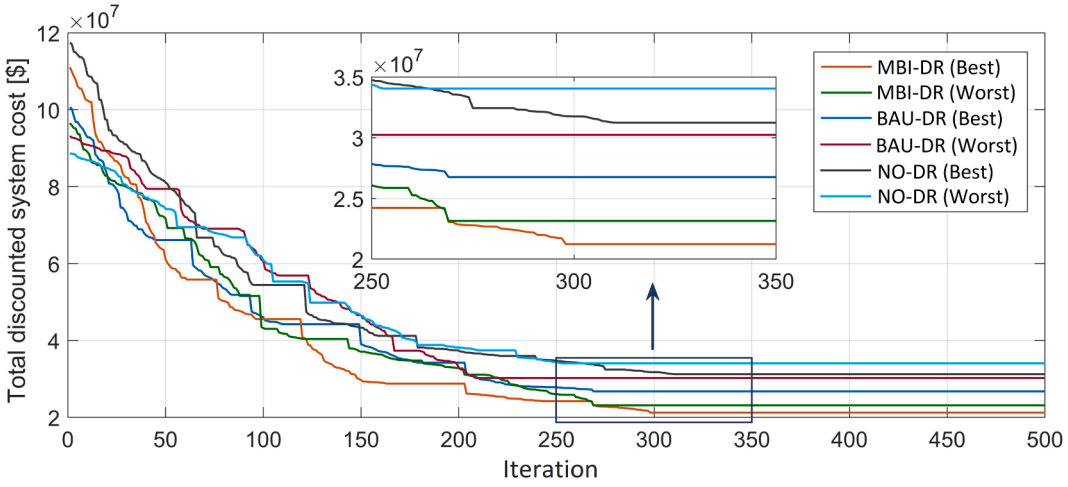

Fig. 14. Convergence process of the MFOA in its best and worst runs throughout 30 simulation cases.

Furthermore, the results summarised in Tables 9 and 10 are indicative of the high efficiency of the proposed model for the aggregator-activated, responsive load-aware MG capacity design in the following ways:

1. While the total discounted equipment-related costs in the BAU case are higher by ~20% than the MBI case, the total discounted income derived from electricity exports has remained at nearly the same level. This is because the majority of this extra cost is spent on the backup power equipment, the energy output of which, according to the MG's hourly operational strategy in Fig. 5, cannot be sold to the main grid–for energy efficiency considerations. To examine the robustness of this assumption, a further unreported model was run in both the MBI and BAU simulation cases, where the backup power was allowed to be sold into the utility grid, while maintaining the rest of the model unchanged. A comparative analysis of the results of the two models for the investigated test-case is presented in Supplementary Material (Additional File 4: Table S1). The results show that the relative difference of the total discounted equipment-related costs in the MBI and BAU cases reduces to ~15%, from ~20% for the base-case model, when the sale of backup power into the grid is not prohibited. The key factor underpinning this change is that the unreported optimisation model that supports the sale of backup power to the main grid finds the opportunity to arbitrage intertemporal differences in wholesale prices and buy-back rates. The unreported model, therefore, increases the proportion of total nominal storage to generation capacity in the optimal equipment capacity configuration as compared to the base-case model. More specifically, the proportion of the share of the total back-up components' capacity to the share of the total primary generation components' capacity in the system's whole-life cost increases from 1.97 and 1.85 to 3.51 and 3.22 in the MBI and BAU model realisations, respectively, at relatively modest extra total equipment-related costs–that is, ~9% and ~5%, respectively. This, however, increases the MG's total net income from the exchange of energy with the utility grid by ~76% and ~429%, respectively, in the aforementioned two cases. As a consequence, the MG's whole-life cost reduces by ~3% and ~5%, respectively, in the two cases mentioned above–but at the cost of higher total energy dissipated as a result of increased energy conversion rocesses.
2. The total discounted income derived from electricity exports in the non-DR-integrated case is higher by ~23% in comparison with the base case, which is mainly due to the increased excess of renewable energy generation in low-demand periods. Note that the export of energy is seen merely as a means to avoid spillage of non-dispatchable renewable energy, and the low export tariff makes it irrational for the solution algorithm to optimise the capacity of the MG equipment for energy export purposes. It should not be overlooked, however, that energy export made a fair contribution to the cost-efficiency of the proposed MG system in all of the cases studied. It is also important to note that the solution algorithm, in the MBI case, has almost always avoided buying and storing electricity from the upstream grid at times of low demand, but the surplus renewable energy is sold to the grid at these times due to: (1) the higher level of feed-in-tariff than the system's levelised cost of energy (LCOE) at most of the off-peak times of the year, and (2) the fact that the battery and SC banks soon reach their maximum capacity limits when the MG system is lightly loaded. This is while the total discounted cost of electricity imports occupies ~10% and ~24% of the total discounted system costs in the BAU DR-integrated and non-DR-integrated cases, respectively.
3. In all of the investigated cases, the optimised size of the electrolyser unit is considerably lower compared to those in established size combinations–of electrolyser to hydrogen reservoir to fuel cell–in the literature (see, for example, [124,125,126]). This is due to the specific conditions of the case study site, where load demand is subject to a high degree of seasonality. Accordingly, an electrolyser of lower capacity is sufficient for the purpose–since the hydrogen tank can be filled gradually during the low season, from October through June. That is also why the optimum capacity of the electrolyser experienced the least changes among the backup power equipment in the three scenarios investigated.
4. As planned, the fuel cell generation using the stored hydrogen has accounted for seasonal load levelling. The optimal capacity of the fuel cell is more highly impacted by the proposed interruptible DR implementation as compared to the battery and SC banks. This observation implies that peak load shaving–fulfilled by exploiting the responsive loads–has had a substantial role in smoothing out the seasonal variation in load demand, and, in turn, improving the load factor of the annual load power demand profile. In other words, much of the suggested DR scheduling strategy's positive impact on the cost-efficiency of the conceptualised MG is derived from its implementation in the winter high season. This also explains the marked increase in the size of the WT, hydrogen tank, fuel cell, and the electrical loads' inverter–as the main drivers of increasing the equipment-related costs–when the DR is implemented in a BAU manner, or, more significantly, when no DR scheduling process is implemented. To provide a clearer picture of the impact of the proposed DSM model on the load power demand data fed into the optimal capacity planning algorithm, the monthly mean 24-h

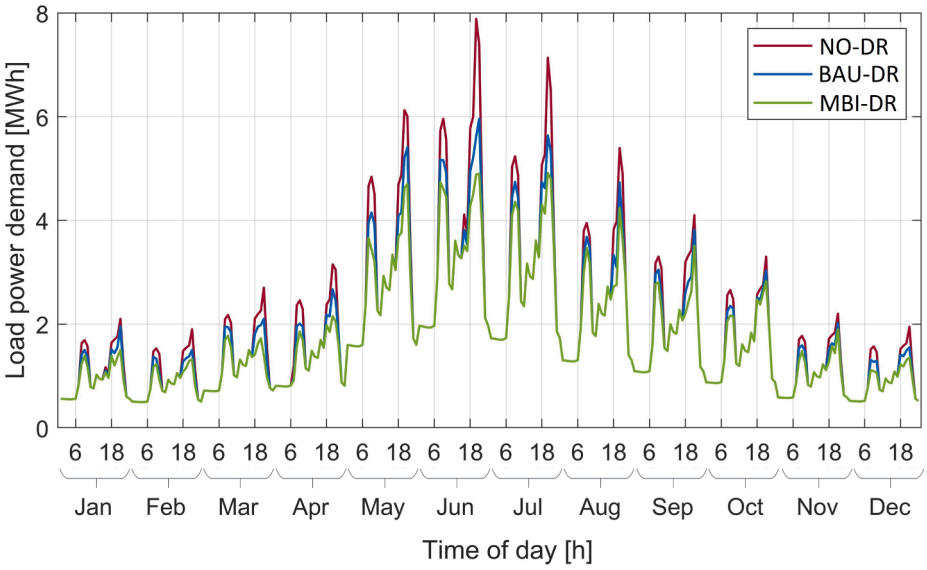

Fig. 15. Comparison of the monthly mean daily profile for load power demand in different simulation cases.

electricity consumption profile is presented in Fig. 15 for the simulation cases under study. According to the figure, realising the proposed DSM model under the BAU and MBI cases shaves ~24% and ~38% off the maximum peak power demand compared to the NO-DR case, respectively. This, consequently, increases the load factor from 0.25 in the NO-DR case to 0.31 and 0.35 in the BAU and MBI simulation cases, respectively.

5. The relatively low share of biomass in the optimised energy resource mix, in spite of its vast potential in the site under study (see Fig. 11), is revealing in two ways: (1) the solution algorithm has succeeded in restricting the bioenergy use to a sustainable level by imposing an emission penalty and, more importantly, (2) it gives credence to the idea that biomass resources need to be deployed in a way that contributes primarily to energy security–in favour of a deep green approach to renewable energy system planning [127]. More specifically, the biopower plant in the conceptualised MG plays a critical role in improving the system's self-sufficiency, as it is the only dispatchable power generation unit in the system.

5.3.1. Financial appraisal

To demonstrate the financial sustainability of the long-term investment proposal, this sub-section compares the LCOE of the MG with the existing retail electricity prices at the site, as well as the LCOE reported in the literature for the most similar projects. More specifically, the project was benchmarked against the studies in the literature that met the following three criteria: (1) a self-sufficiency ratio of at least 85% if the system is grid-connected, (2) powered by 100% renewable energy, and (3) tailored to the electrification of small- to medium-scale communities.

The LCOE, in the MG context, represents the average revenue per unit of energy generated that would be required to recoup the lifetime costs of the system. Accordingly, the LCOE [$/kWh] of the MG under study can be calculated as follows [128]:

$$LCOE = \frac{WLC}{\sum_{n=1}^{PL} \frac{(\sum_{t=1}^{8760} P_L(t) + \sum_{t=1}^{8760} P_S(t))\Delta t}{(1+ir)^n}}, \tag{49}$$

where PL represents the project lifetime [years], ir denotes the real interest rate per annum [%], and the terms $\sum_{t=1}^{8760} P_L(t)$ and $\sum_{t=1}^{8760} P_S(t)$ respectively denote the total annual electric and hydrogen power demand on the MG, which are discounted to reflect the NPV of future energy flows.

By solving Eq. (49), the LCOE of the proposed MG is found to be $0.08/kWh, while the most recent yearly average retail price of electricity is as high as $0.22/kWh at the studied site. That is, implementing the proposed MG system is expected to realise savings of at least 64% in the community's energy costs if financed as a community-owned renewable energy project. Note that the MG's LCOE is calculated for the case where the aggregator-mediated demand-side flexibility resources are scheduled using the proposed non-cooperative game-theoretic DSM framework–and the whole-life cost of the MG is $21.72 m. Table 11 benchmarks the conceptualised system in terms of the LCOE with the most similar projects in the literature.

As can be seen from Table 11, the LCOE of the simulated MG is highly competitive with that of the best value reported in the recent literature for a community-scale, 100%-renewable electrification project. Add to this the fact that a carbon-free, hydrogen-based, light-duty transportation fleet is integrated into the proposed MG, making it one of the first of its kind. This provides additional support for the economic sustainability of the conceptualised community energy system.

Based on the above premises, the modelled MG provides an evidence base to inform the energy sector and climate change policy, infrastructure providers, and the wider modelling community of both the technical feasibility and economic viability of leveraging the potential synergies in the integration of energy networks for electricity, heating, and transport to realise economy-wide deep decarbonisation.

6. Conclusions

The projections on the uptake of demand response programmes used in the long-term capital infrastructure planning of sustainable energy systems are substantially influenced by the biases and preferences of end-consumers, which can be modelled in terms of the elasticity of the customer supply of demand response capacity. This study, one of the first to provide an understanding of end-consumer behavioural traits in long-term demand-side management schemes, developed a comfort-aware, demand response-integrated optimisation model for equipment capacity-planning of renewable energy systems. To this end, the study developed a two-stage, aggregator-mediated, non-cooperative game-theoretic demand-side management market design to improve the accuracy of the long-term forecasts of end-users' participation in incentive-directed demand response programmes. The proposed model provides an effective framework for improving the accuracy of

Table 11
Comparative evaluation of the proposed MG's LCOE against those of the comparable schemes.

Reference	Renewable energy system architecture	Case study site(s)	Climatic conditions	Unsubsidised LCOE [$/kWh][*, †]
Hosseinalizadeh et al., 2016 [129]	An on-grid PV/WT/BESS/FC MG	Four villages in Iran, namely Moaleman, Ghadamgah, Marvdasht, and Nikouyeh	Diverse climatic conditions	0.54–1.60
Shang et al., 2016 [130]	An insular PV/WT/BESS/DG MG	An unnamed island near Singapore	Tropical/equatorial	0.14
Chauhan and Saini, 2017 [28]	A stand-alone PV/WT/BESS/DG/BP/MHPP MG	Chamoli district, Uttarakhand state, India	Warm temperate	0.07–0.10
Fu et al., 2018 [131]	Stand-alone solar PV systems	U.S.-wide	Diverse climatic conditions	0.13–0.16
Li, 2019 [132]	A grid-independent PV/BESS/FC MG	A community centre in Kunming, China	Humid subtropical	1.55
Rezk et al., 2019 [133]	A grid-independent PV/FC hybrid renewable energy system	The city of Minya, Egypt	Mediterranean	0.06
This study	A grid-tied PV/WT/MHPP/BP/FC/BESS/SC MG	The town of Ohakune, New Zealand	Temperate	0.08

Key: BESS = Battery Energy Storage System, BP = Biopower Plant, DG = Diesel Generator, FC = Fuel Cell, LCOE = Levelised Cost of Energy, MG = Micro-Grid, MHPP = Micro-Hydro Power Plant, PV = Photovoltaic, SC = Super-Capacitor, WT = Wind turbine.
† Where appropriate, the LCOE values were adjusted to 2019 U.S. dollars.
* For cases where different configurations of the proposed system are investigated, or the conceptualised system is optimised under different climatic conditions, or the optimisation process is carried out in a multi-objective search space or in a stochastic way, the value of LCOE is reported as a range, rather than a certain value.

investment assessments made for demand response-aided energy systems by adopting the endogenous Stackelberg leader–follower relationships in two stages, namely: first, for interactions between the micro-grid operator and responsive load aggregators, and second, for aggregator-customer exchanges. Moreover, the devised model successfully generalised the long-term, community-level renewable energy system design problem in the following four areas:

1. It guaranteed a level playing field for a variety of clean energy technologies–in the interest of energy diversification–where the use of biomass resources is limited to a sustainable level by imposing a new constraint term.
2. It implemented the potential of cross-vector integration (in particular, power-to-gas technology) in conjunction with the value of fuel cell electric vehicles in vehicle-to-grid operation to improve the flexibility of energy systems with deep penetration of renewables.
3. It allowed for a *meta*-heuristic solution algorithm based on the moth-flame optimisation algorithm to find the cost-optimal mix of micro-grid assets, whilst facilitating long-term decision-making on the delivery of aggregator-mediated incentive-responsive loads using a realistic example. The use of a case study illustrated the application of the model in the town of Ohakune, New Zealand, demonstrating that many of the challenges for integrating a 100%-renewable energy system can be surmounted.
4. The suggested solution algorithm was also shown to be efficient in nearing the formulated problem's globally optimum solution. In addition, a comparative analysis of the proposed market-driven and business-as-usual realisations of the interruptible load programme verified the validity of the proposed modelling framework as a decision support tool for utilities to make reliable forecasts about the engagement of different classes of end-consumers in demand response programmes. This is particularly important when designing greenfield renewable energy systems, or as micro-grids are used to increase the penetration of responsive loads.

The numeric results obtained from the model's application to the test-case system of Ohakune have revealed two novel insights:

1. The use of the proposed two-stage demand-side management market design for the projection of flexible demand resources brings higher-order information about micro-grid operator-aggregators-customers interactions into the analysis, which can be leveraged towards improving the economic viability of renewable energy systems. Notably, as compared to the case where demand-side resources are managed using a business-as-usual interruptible load approach, the model results have indicated that a cost saving of at least 21% (equating to approximately $5.5 m) can be generated for the simulated micro-grid in Ohakune, while imposing the same discomfort cost on end-users.
2. The large-scale supply of demand-side flexibility resources, enabled by demand response aggregators, has great potential in reducing the estimated life-cycle cost of sustainable energy systems. Specifically, the evidence from this study demonstrates that assisting the conceptualised micro-grid with incentive-driven, market-directed demand-side management processes reduces the total discounted system costs by circa 32% (equating to around $10 m in this case study). In this light, a thorough analysis of the value of lost load to the target customers–in the interest of improving the accuracy of the forecasted willingness of the end-users to deliver their demand response resources–is of paramount importance in the design phase of all-renewable micro-grids. This is especially true for the development of first-access energy systems in remote areas where the values of unserved energy are expected to be lower than those estimated for urban and industrial customers.

In conclusion, this paper has shown that capturing the flexible demand potential of small- to medium-scale customers during the planning phases of a hydrogen-based grid-connected micro-grid system can pave the way toward achieving greater energy independence, energy democracy, and energy security in rural and semi-urban areas in a cost-effective and environmentally efficient way.

CRediT authorship contribution statement

Soheil Mohseni: Conceptualization, Methodology, Data curation, Formal analysis, Investigation, Resources, Software, Validation, Visualization, Writing - original draft. **Alan C. Brent:** Supervision, Project administration, Writing - review & editing. **Scott Kelly:** Supervision, Writing - review & editing. **Will N. Browne:** Supervision, Writing - review & editing. **Daniel Burmester:** Supervision, Writing - review & editing.

Declaration of Competing Interest

The authors declare that they have no known competing financial interests or personal relationships that could have appeared to influence the work reported in this paper.

Acknowledgements

The authors would like to acknowledge excellent comments and suggestions on the categorisation of load demand from the audience of the 2020 17th International Conference on the European Energy Market (EEM) in Stockholm, Sweden, as well as constructive comments from the anonymous reviewers.

Appendix A. Supplementary material

Supplementary data to this article can be found online at https://doi.org/10.1016/j.apenergy.2021.116563.

References

[1] Hui H, Ding Y, Shi Q, Li F, Song Y, Yan J. 5G network-based Internet of Things for demand response in smart grid: a survey on application potential. Appl Energy 2020;257:113972. https://doi.org/10.1016/j.apenergy.2019.113972.
[2] Mohseni S, Moghaddas-Tafreshi SM. A multi-agent system for optimal sizing of a cooperative self-sustainable multi-carrier microgrid. Sustain Cities Soc 2018;38:452–65. https://doi.org/10.1016/j.scs.2018.01.016.
[3] Niu J, Tian Z, Zhu J, Yue L. Implementation of a price-driven demand response in a distributed energy system with multi-energy flexibility measures. Energy Convers Manag 2020;208:112575. https://doi.org/10.1016/j.enconman.2020.112575.
[4] Ihsan A, Jeppesen M, Brear MJ. Impact of demand response on the optimal, techno-economic performance of a hybrid, renewable energy power plant. Appl Energy 2019;238:972–84. https://doi.org/10.1016/j.apenergy.2019.01.090.
[5] Modarresi Ghazvini A, Olamaei J. Optimal sizing of autonomous hybrid PV system with considerations for V2G parking lot as controllable load based on a heuristic optimization algorithm. Sol Energy 2019;184:30–9. https://doi.org/10.1016/j.solener.2019.03.087.
[6] Jing Z, Zhu J, Hu R. Sizing optimization for island microgrid with pumped storage system considering demand response. J Mod Power Syst Clean Energy 2018;6(4):791–801. https://doi.org/10.1007/s40565-017-0349-1.
[7] Kim H, Bae J, Baek S, Nam D, Cho H, Chang HJ. Comparative analysis between the Government Micro-Grid Plan and computer simulation results Based on real data: the practical case for a South Korean Island. Sustainability 2017;9(2):197. https://doi.org/10.3390/su9020197.
[8] Amir V, Azimian M. Dynamic multi-carrier microgrid deployment under uncertainty. Appl Energy 2020;260:114293. https://doi.org/10.1016/j.apenergy.2019.114293.
[9] Gelazanskas L, Gamage KAA. Demand side management in smart grid: a review and proposals for future direction. Sustain Cities Soc 2014;11:22–30. https://doi.org/10.1016/j.scs.2013.11.001.
[10] Haider HT, See OH, Elmenreich W. A review of residential demand response of smart grid. Renew Sustain Energy Rev 2016;59:166–78. https://doi.org/10.1016/j.rser.2016.01.016.
[11] Esther BP, Kumar KS. A survey on residential Demand Side Management architecture, approaches, optimization models and methods. Renew Sustain Energy Rev 2016;59:342–51. https://doi.org/10.1016/j.rser.2015.12.282.
[12] Wang J, Zhong H, Ma Z, Xia Q, Kang C. Review and prospect of integrated demand response in the multi-energy system. Appl Energy 2017;202:772–82. https://doi.org/10.1016/j.apenergy.2017.05.150.
[13] Robert FC, Sisodia GS, Gopalan S. A critical review on the utilization of storage and demand response for the implementation of renewable energy microgrids. Sustain Cities Soc 2018;40:735–45. https://doi.org/10.1016/j.scs.2018.04.008.
[14] Jordehi AR. Optimisation of demand response in electric power systems, a review. Renew Sustain Energy Rev 2019;103:308–19. https://doi.org/10.1016/j.rser.2018.12.054.
[15] Behrangrad M. A review of demand side management business models in the electricity market. Renew Sustain Energy Rev 2015;47:270–83. https://doi.org/10.1016/j.rser.2015.03.033.
[16] Jin X, Wu Q, Jia H. Local flexibility markets: literature review on concepts, models and clearing methods. Appl Energy 2020;261:114384. https://doi.org/10.1016/j.apenergy.2019.114387.
[17] Kahrobaee S, Asgarpoor S, Qiao W. Optimum sizing of distributed generation and storage capacity in smart households. IEEE Trans Smart Grid 2013;4(4):1791–801. https://doi.org/10.1109/TSG.2013.2278783.
[18] Yu L, Li YP, Huang GH, An CJ. A robust flexible-probabilistic programming method for planning municipal energy system with considering peak-electricity price and electric vehicle. Energy Convers Manag 2017;137:97–112. https://doi.org/10.1016/j.enconman.2017.01.028.
[19] Varasteh F, Nazar MS, Heidari A, Shafie-khah M, Catalão JPS. Distributed energy resource and network expansion planning of a CCHP based active microgrid considering demand response programs. Energy 2019;172:79–105. https://doi.org/10.1016/j.energy.2019.01.015.
[20] Cardoso G, Stadler M, Bozchalui MC, Sharma R, Marnay C, Barbosa-Póvoa A, et al. Optimal investment and scheduling of distributed energy resources with uncertainty in electric vehicle driving schedules. Energy 2014;64:17–30. https://doi.org/10.1016/j.energy.2013.10.092.
[21] Hosseinnia H, Nazarpour D, Talavat V. Multi-objective optimization framework for optimal planning of the microgrid (MG) under employing demand response program (DRP). J Ambient Intell Humaniz Comput 2019;10(7):2709–30. https://doi.org/10.1007/s12652-018-0977-y.
[22] Moghaddas-Tafreshi SM, Jafari M, Mohseni S, Kelly S. Optimal operation of an energy hub considering the uncertainty associated with the power consumption of plug-in hybrid electric vehicles using information gap decision theory. Int J Electr Power Energy Syst 2019;112:92–108. https://doi.org/10.1016/j.ijepes.2019.04.040.
[23] Martins VF, Borges CLT. Active distribution network integrated planning incorporating distributed generation and load response uncertainties. IEEE Trans Power Syst 2011;26(4):2164–72. https://doi.org/10.1109/TPWRS.2011.2122347.
[24] Zhu L, Yan Z, Lee WJ, Yang X, Fu Y, Cao W. Direct load control in microgrids to enhance the performance of integrated resources planning. IEEE Trans Ind Appl 2015;51(5):3553–60. https://doi.org/10.1109/TIA.2015.2413960.
[25] Atia R, Yamada N. Sizing and analysis of renewable energy and battery systems in residential microgrids. IEEE Trans Smart Grid 2016;7(3):1204–13. https://doi.org/10.1109/TSG.2016.2519541.
[26] Pazouki S, Haghifam MR. Optimal planning and scheduling of energy hub in presence of wind, storage and demand response under uncertainty. Int J Electr Power Energy Syst 2016;80:219–39. https://doi.org/10.1016/j.ijepes.2016.01.044.
[27] Schachter JA, Mancarella P, Moriarty J, Shaw R. Flexible investment under uncertainty in smart distribution networks with demand side response: assessment framework and practical implementation. Energy Policy 2016;97:439–49. https://doi.org/10.1016/j.enpol.2016.07.038.
[28] Chauhan A, Saini RP. Size optimization and demand response of a stand-alone integrated renewable energy system. Energy 2017;124:59–73. https://doi.org/10.1016/j.energy.2017.02.049.
[29] Nojavan S, Majidi M, Esfetanaj NN. An efficient cost-reliability optimization model for optimal siting and sizing of energy storage system in a microgrid in the presence of responsible load management. Energy 2017;139:89–97. https://doi.org/10.1016/j.energy.2017.07.148.
[30] Amrollahi MH, Bathaee SMT. Techno-economic optimization of hybrid photovoltaic/wind generation together with energy storage system in a stand-alone micro-grid subjected to demand response. Appl Energy 2017;202:66–77. https://doi.org/10.1016/j.apenergy.2017.05.116.
[31] Chen J, Zhang W, Li J, Zhang W, Liu Y, Zhao B, et al. Optimal sizing for grid-tied microgrids with consideration of joint optimization of planning and operation. IEEE Trans Sustain Energy 2018;9(1):237–48. https://doi.org/10.1109/TSTE.2017.2724583.
[32] Zheng Y, Jenkins BM, Kornbluth K, Kendall A, Træholt C. Optimization of a biomass-integrated renewable energy microgrid with demand side management under uncertainty. Appl Energy 2018;230:836–44. https://doi.org/10.1016/j.apenergy.2018.09.015.
[33] Xiao H, Pei W, Dong Z, Kong L. Bi-level planning for integrated energy systems incorporating demand response and energy storage under uncertain environments using novel metamodel. CSEE J Power Energy Syst 2018;4(2):155–67. https://doi.org/10.17775/CSEEJPES.2017.01260.
[34] Husein M, Chung I-Y. Optimal design and financial feasibility of a university campus microgrid considering renewable energy incentives. Appl Energy 2018;225:273–89. https://doi.org/10.1016/j.apenergy.2018.05.036.
[35] Gazijahani FS, Salehi J. Reliability constrained two-stage optimization of multiple renewable-based microgrids incorporating critical energy peak pricing demand response program using robust optimization approach. Energy 2018;161:999–1015. https://doi.org/10.1016/j.energy.2018.07.191.
[36] Amir V, Jadid S, Ehsan M. Optimal planning of a multi-carrier microgrid (MCMG) considering demand-side management. Int J Renew Energy Res 2018;8(1):238–49.
[37] Mohseni S, Brent A, Burmester D, Chatterjee A. Optimal sizing of an islanded micro-grid using meta-heuristic optimization algorithms considering demand-side management. In: Proceedings of the 2018 Australas. Univ. Power Eng. Conf., Auckland, New Zealand, 27–30 Nov. 2018, p. 1–6. https://doi.org/10.1109/AUPEC.2018.8757882.
[38] Nazari A, Keypour R. A two-stage stochastic model for energy storage planning in a microgrid incorporating bilateral contracts and demand response program. J Energy Storage 2019;21:281–94. https://doi.org/10.1016/j.est.2018.12.002.
[39] Prathapaneni DR, Detroja KP. An integrated framework for optimal planning and operation schedule of microgrid under uncertainty. Sustain Energy, Grids Networks 2019;19:100232. https://doi.org/10.1016/j.segan.2019.100232.
[40] Bhamidi L, Sivasubramani S. Optimal planning and operational strategy of a residential microgrid with demand side management. IEEE Syst J, Early Access 2019:1–9. https://doi.org/10.1109/JSYST.2019.2918410.
[41] Mohseni S, Brent AC, Burmester D. A demand response-centred approach to the long-term equipment capacity planning of grid-independent micro-grids optimized by the moth-flame optimization algorithm. Energy Convers Manag 2019;200:112105. https://doi.org/10.1016/j.enconman.2019.112105.
[42] Salyani P, Abapour M, Zare K, Babri T. Optimal stochastic planning of DERs in a game theory framework considering demand response and pollution issues. In: Demand Response Application in Smart Grids: Concepts and Planning Issues, Volume 1. Cham: Springer International Publishing; 2020. p. 193–214. https://doi.org/10.1007/978-3-030-31399-9_8.
[43] Burger S, Chaves-Avila JP, Batlle C, Perez-Arriaga IJ. The Value of Aggregators in Electricity Systems. CEERP WP 2016-001. MIT Center for Energy and Environmental Policy Research; 2016. Available: https://energy.mit.edu/

wp-content/uploads/2016/01/CEEPR_WP_2016-001.pdf [Accessed: 18-Oct.-2020].
[44] Stevenson T, Batstone S, Reeve D, Poynton M, Comendant C. Transitioning to zero net emissions by 2050: moving to a very low-emissions electricity system in New Zealand. SAPERE Research Group – Prepared for the New Zealand Productivity Commission; 2018. Available: https://www.productivity.govt.nz/assets/Documents/3374eca8c4/Transitioning-to-zero-net-emissions-by-2050.pdf [Accessed: 18-Oct.2020].
[45] Okur Ö, Voulis N, Heijnen P, Lukszo Z. Aggregator-mediated demand response: minimizing imbalances caused by uncertainty of solar generation. Appl Energy 2019;247:426–37. https://doi.org/10.1016/j.apenergy.2019.04.035.
[46] Nash J. Non-cooperative games. Ann Math 1951;54(2):286–95. https://doi.org/10.2307/1969529.
[47] Basar T, Olsder GJ. Dynamic noncooperative game theory, vol. 23. Siam; 1999.
[48] Canadian Solar Inc. CS6K-270|275|280P; Dec. 2017, PV Module Product Datasheet V5.552_EN. Available: https://www.collectiu-solar.cat/pdf/2-Panel-Canadian_Solar-Datasheet-CS6K.pdf [Accessed: 4-Mar.-2020].
[49] Patel MR. Wind and solar power systems: design, analysis, and operation. CRC Press; 2005.
[50] Murugaperumal K, Raj PADV. Feasibility design and techno-economic analysis of hybrid renewable energy system for rural electrification. Sol Energy 2019;188:1068–83. https://doi.org/10.1016/j.solener.2019.07.008.
[51] Meteonorm. Bern, Switzerland: Genossenschaft Meteotest; 2018. Version 7.3.0.
[52] Alstom. ecotècnia ECO 48/750; Aug. 2014, ecotècnia ECO 48/750 Datasheet. [Online]. Available: https://en.wind-turbine-models.com/turbines/791-ecot-cnia-eco-48-750#datasheet/ [Accessed: 4-Mar.-2020].
[53] Wagner R, Antoniou I, Pedersen SM, Courtney MS, Jørgensen HE. The influence of the wind speed profile on wind turbine performance measurements. Wind Energy Int J Prog Appl Wind Power Convers Technol 2009;12(4):348–62.
[54] Gipe P. Wind power. Wind Eng 2004;28(5):629–31. https://doi.org/10.1260/0309524043028145.
[55] Sunceo Hydro. XJ50-100SCTF6-Z; 2015. [Online]. Available: https://www.micro-hydro-power.com/100kw-hydro-turbine-generator/ [Accessed: 4-Mar.-2020].
[56] Khan MRB, Jidin R, Pasupuleti J. Multi-agent based distributed control architecture for microgrid energy management and optimization. Energy Conserv Manag 2016;112:288–307. https://doi.org/10.1016/j.enconman.2016.01.011.
[57] Bosona T, Gebresenbet G. Modeling hydropower plant system to improve its reservoir operation. Int J Water Resour Environ Eng 2 (4):87–94. [Online]. Available: https://academicjournals.org/journal/IJWREE/article-full-text-pdf/3424C7E1713 [Accessed: 19-Dec.-2020].
[58] All Power Labs. Old PP20 vs New PP30 Cogen-CS: Technical Specifications & Comparisons; Jan. 2019, Rev 03. Available: http://www.allpowerlabs.com/wp-content/uploads/2019/07/PP30-vs-PP20-Spec-Sheet-Public-2019-Rev-03-current-July-2019.pdf [Accessed: 4-Mar.-2020].
[59] Singh S, Singh M, Kaushik SC. Feasibility study of an islanded microgrid in rural area consisting of PV, wind, biomass and battery energy storage system. Energy Convers Manag 2016;128:178–90. https://doi.org/10.1016/j.enconman.2016.09.046.
[60] Ahmed OY, Ries MJ, Northrop WF. Emissions factors from distributed, small-scale biomass gasification power generation: Comparison to open burning and large-scale biomass power generation. Atmos Environ 2019;200:221–7. https://doi.org/10.1016/j.atmosenv.2018.12.024.
[61] Moghaddas-Tafreshi SM, Mohseni S, Karami ME, Kelly S. Optimal energy management of a grid-connected multiple energy carrier micro-grid. Appl Therm Eng 2019;152:796–806. https://doi.org/10.1016/j.applthermaleng.2019.02.113.
[62] Qin H, Kimball JW. Solid-state transformer architecture using AC-AC dual-active-bridge converter. IEEE Trans Ind Electron 2013;60(9):3720–30. https://doi.org/10.1109/TIE.2012.2204710.
[63] Leonics Co. Apollo GTP-500; 2018, P.LEN.BRO.INV.156 Rev. 12.00. Available: http://www.leonics.com/product/renewable/inverter/dl/GTP-500-156.pdf [Accessed: 4-Mar.-2020].
[64] Akram U, Khalid M, Shafiq S. An innovative hybrid wind-solar and battery-supercapacitor microgrid system—development and optimization. IEEE Access 2017;5:25897–912. https://doi.org/10.1109/ACCESS.2017.2767618.
[65] Eaton Corporation. XLR-48 Supercapacitor; Feb. 2019, Technical Data 10510. Available: https://datasheet.octopart.com/XLR-48R6167-R-Eaton-datasheet-130052459.pdf [Accessed: 4-Mar.-2020].
[66] CellCube Energy Storage Systems Inc. Use your own power grid: Intelligent storage systems based on vanadium redox flow technology; 2018, D6144/0714ND3. Available: https://static1.squarespace.com/static/5b1198ada2772c6585959926/t/5b57363f88251b71261fc4a1/1532442177499/CellCube+-+Use+Your+Own+Power+Grid.pdf [Accessed: 4-Mar.-2020].
[67] H-TEC Systems. The core of electrolysis: PEM electrolyser stacks – Designed for ideal integration in systems; 2019, H-TEC Series-S: S 30/30. Available: https://www.h-tec-systems.com/fileadmin/Content/PDFs/19022019/H-TEC_SYSTEMS_Datenblatt_Stacks_SE30_30_EN.PDF [Accessed: 4-Mar.-2020].
[68] Ballard Power Systems Inc. FCgen–1020ACS; May 2015, SPC5101559-0H. Available: https://www.ballard.com/docs/default-source/spec-sheets/fcgen-1020-acs-v2.pdf?sfvrsn=c3ebc380_4 [Accessed: 19-Dec.-2020].
[69] Graham JDT, Mulvenna AJ, Mufford WE, Borck JG, Ko J, Harper MAM. Hydrogen fueling station. U.S. Patent 6,810,925, issued 2 Nov. 2004.
[70] Pure Energy Centre Limited. Hydrogen fueling station; 2019. [Online]. Available: https://pureenergycentre.com/hydrogen-fueling-station/ [Accessed: 4-Mar.-2020].
[71] Takagi H. Queueing analysis: a foundation of performance evaluation. Amsterdam: North-Holland; 1991.
[72] Robledo CB, Oldenbroek V, Abbruzzese F, van Wijk AJM. Integrating a hydrogen fuel cell electric vehicle with vehicle-to-grid technology, photovoltaic power and a residential building. Appl Energy 2018;215:615–29. https://doi.org/10.1016/j.apenergy.2018.02.038.
[73] Ahmad MS, Mehmood MA, Luo H, Shen B, Latif M, Ghani WAWAK, et al. Pyrolysis and thermogravimetric study to elucidate the bioenergy potential of novel feedstock produced on poor soils while keeping the environmental sustainability intact. Sustain 2019;11(13). https://doi.org/10.3390/su11133592.
[74] Winter C-J, Sizmann RL, Vant-Hull LL, editors. Solar power plants: fundamentals, technology, systems, economics. Springer Science & Business Media; 2012.
[75] My Solar Quotes. Solar Power Buy-Back Rates; 2020. [Online]. Available: https://www.mysolarquotes.co.nz/about-solar-power/residential/solar-power-buy-back-rates-nz/ [Accessed: 4-Mar.-2020].
[76] [dataset] CliFlo: New Zealand's National Climate Database. [Online]. Available: http://cliflo.niwa.co.nz/ [Retrieved: 10-Oct.-2019].
[77] Elert G. Energy density of hydrogen. Energy Density of Hydrogen—The Physics Factbook 2017;22.
[78] XiaoW, Dunford WG, Capel A. A novel modeling method for photovoltaic cells. In: Proceedings of the 2004 IEEE 35th Annual Power Electronics Specialists Conference (IEEE Cat. No.04CH37551), Aachen, Germany, 20–25 Jun. 2004, pp. 1950–56. https://doi.org/10.1109/PESC.2004.1355416.
[79] Engineering ToolBox. Wind Shear; 2008. [Online]. Available: https://www.engineeringtoolbox.com/wind-shear-d_1215.html/ [Accessed: 4-Mar.-2020].
[80] Interagency Working Group on Social Cost of Greenhouse Gases, United States Government. Technical support document: technical update of the social cost of carbon for regulatory impact analysis under executive order 12866. The August 2016 revision of the 2013 Technical Support Document on the Social Cost of Carbon. Available: https://www.epa.gov/sites/production/files/2016-12/documents/sc_co2_tsd_august_2016.pdf [Accessed: 4-Mar.-2020].
[81] Nerini FF, Broad O, Mentis D, Welsch M, Bazilian M, Howells M. A cost comparison of technology approaches for improving access to electricity services. Energy 2016;95:255–65. https://doi.org/10.1016/j.energy.2015.11.068.
[82] Thomas D, Deblecker O, Ioakimidis CS. Optimal design and techno-economic analysis of an autonomous small isolated microgrid aiming at high RES penetration. Energy 2016;116:364–79. https://doi.org/10.1016/j.energy.2016.09.119.
[83] Duman AC, Güler Ö. Techno-economic analysis of off-grid PV/wind/fuel cell hybrid system combinations with a comparison of regularly and seasonally occupied households. Sustain Cities Soc 2018;42:107–26. https://doi.org/10.1016/j.scs.2018.06.029.
[84] Mohseni S, Brent AC. Economic viability assessment of sustainable hydrogen production, storage, and utilisation technologies integrated into on- and off-grid micro-grids: a performance comparison of different meta-heuristics. Int J Hydrogen Energy 2019. https://doi.org/10.1016/j.ijhydene.2019.11.079.
[85] Oldenbroek V, Smink G, Salet T, van Wijk AJM. Fuel cell electric vehicle as a power plant: Techno-economic scenario analysis of a renewable integrated transportation and energy system for smart cities in two climates. Appl Sci 2020;10(1):143. https://doi.org/10.3390/app10010143.
[86] Oldenbroek V, Hamoen V, Alva S, Robledo CB, Verhoef LA, van Wijk AJM. Fuel cell electric vehicle-to-grid: experimental feasibility and operational performance as balancing power plant. Fuel Cells 2018;18(5):649–62. https://doi.org/10.1002/fuce.201700192.
[87] Farahani SS, van der Veen R, Oldenbroek V, Alavi F, Lee EHP, van de Wouw N, et al. A hydrogen-based integrated energy and transport system: the design and analysis of the car as power plant concept. IEEE Trans Syst Man Cybern Mag 2019;5(1):37–50. https://doi.org/10.1109/MSMC.2018.2873408.
[88] Steward DM. Critical Elements of Vehicle-to-Grid (V2G) Economics. No. NREL/TP-5400-69017, Golden, CO, USA: National Renewable Energy Lab (NREL); 2017.
[89] Soshinskaya M, Crijns-Graus WHJ, van der Meer J, Guerrero JM. Application of a microgrid with renewables for a water treatment plant. Appl Energy 2014;134:20–34. https://doi.org/10.1016/j.apenergy.2014.07.097.
[90] Khan MRB, Jidin R, Pasupuleti J, Shaaya SA. Optimal combinations of PV, wind, micro-hydro and diesel systems for a seasonal load demand. In: Proceedings of the 2014 IEEE International Conference on Power and Energy (PECon), Kuching, Malaysia, 1–3 Dec. 2014, pp. 171–76. https://doi.org/10.1109/PECON.2014.7062435.
[91] Chauhan A, Saini RP. Techno-economic optimization based approach for energy management of a stand-alone integrated renewable energy system for remote areas of India. Energy 2016;94:138–56. https://doi.org/10.1016/j.energy.2015.10.136.
[92] Naderi M, Bahramara S, Khayat Y, Bevrani H. Optimal planning in a developing industrial microgrid with sensitive loads. Energy Rep 2017;3:124–34. https://doi.org/10.1016/j.egyr.2017.08.004.
[93] Mohseni S, Moghaddas-Tafreshi SM. Development of a multi-agent system for optimal sizing of a commercial complex microgrid. arXiv preprint, arXiv:1811.12553; 2018.
[94] Mohseni S, Moghaddas-Tafreshi SM. A multi-agent approach to optimal sizing of a combined heating and power microgrid. arXiv preprint, arXiv:1812.11076; 2018.
[95] Mohseni S, Brent AC, Burmester D. Community resilience-oriented optimal micro-grid capacity expansion planning: The case of Totarabank eco-village, New Zealand. Energies 13 (15):3970. https://doi.org/10.3390/en13153970.
[96] Mohseni S, Brent AC, Kelly S. A hierarchical, market-based, non-cooperative game-theoretic approach to projecting flexible demand-side resources: towards more realistic demand response-integrated, long-term energy planning models.

In: Proceedings of the 2020 17th International Conference on the European Energy Market (EEM), Stockholm, Sweden, 16–18 Sep. 2020, pp. 1–6. https://doi.org/10.1109/EEM49802.2020.9221977.
[97] Yu M, Hong SH. Incentive-based demand response considering hierarchical electricity market: a Stackelberg game approach. Appl Energy 2017;203:267–79. https://doi.org/10.1016/j.apenergy.2017.06.010.
[98] Fahrioglu M, Alvarado L. Designing incentive compatible contracts for effective demand management. IEEE Trans Power Syst 2000;15(4):1255–60. https://doi.org/10.1109/59.898098.
[99] Fahrioglu M, Alvarado L. Using utility information to calibrate customer demand management behavior models. IEEE Trans Power Syst 2001;16(2):317–22. https://doi.org/10.1109/59.918305.
[100] Mirjalili S. Moth-flame optimization algorithm: a novel nature-inspired heuristic paradigm. Knowledge-Based Syst 2015;89:228–49. https://doi.org/10.1016/j.knosys.2015.07.006.
[101] Goldberg DE, Holland JH. Genetic algorithms and machine learning. Mach Learn 1988;3:95–9. https://doi.org/10.1023/A:1022602019183.
[102] Kennedy J, Eberhart R. Particle swarm optimization. In: Proceedings of the 1995 International Conference on Neural Networks, Perth, WA, Australia, 27 Nov.–1 Dec. 1995, p. 1942–48. https://doi.org/10.1109/ICNN.1995.488968.
[103] Mohseni S, Brent AC, Burmester D. A comparison of metaheuristics for the optimal capacity planning of an isolated, battery-less, hydrogen-based micro-grid. Appl Energy 2020;259:114224. https://doi.org/10.1016/j.apenergy.2019.114224.
[104] Mohseni S, Brent AC, Burmester D. A sustainable energy investment planning model based on the micro-grid concept using recent metaheuristic optimization algorithms. In: Proceedings of the 2019 IEEE Congress on Evolutionary Computation (CEC), Wellington, New Zealand, 10–13 Jun. 2019, pp. 219–26. https://doi.org/10.1109/CEC.2019.8790007.
[105] Mohseni S, Brent AC, Burmester D, Chatterjee A. Stochastic optimal sizing of micro-grids using the moth-flame optimization algorithm. In: Proceedings of the 2019 IEEE Power & Energy Society General Meeting (PESGM), Atlanta, GA, USA, 4–8 Aug. 2019, pp. 1–5. https://doi.org/10.1109/PESGM40551.2019.8973570.
[106] Trading Economics. New Zealand – Real Interest Rate. [Online]. Available: https://tradingeconomics.com/new-zealand/real-interest-rate-percent-wb-data.html/ [Retrieved: 5-Feb.-2020].
[107] Hübert T, Boon-Brett L, Buttner W. Sensors for safety and process control in hydrogen technologies. CRC Press; 2016.
[108] Chen Q, Xia M, Zhou Y, Cai H, Wu J, Zhang H. Optimal planning for partially self-sufficient microgrid with limited annual electricity exchange with distribution grid. IEEE Access 2019;7:123505–20. https://doi.org/10.1109/ACCESS.2019.2936762.
[109] Chowdhury S, Zhang J, Messac A. Avoiding premature convergence in a mixed-discrete particle swarm optimization (MDPSO) algorithm. In: Proceedings of the 53rd AIAA/ASME/ASCE/AHS/ASC Structures, Structural Dynamics and Materials Conference, Honolulu, Hawaii, USA, 23–26 Apr. 2012, p. 1678. https://doi.org/10.2514/6.2012-1678.
[110] Khan B, Singh P. Selecting a meta-heuristic technique for smart micro-grid optimization problem: a comprehensive analysis. IEEE Access 2017;5:13951–77. https://doi.org/10.1109/ACCESS.2017.2728683.
[111] MATLAB. Natick, MA: The MathWorks Inc; 2018. R2018b, Version 9.5.
[112] Anonymous. Ohakune Useful Information; 2011. [Online]. Available: http://www.visitohakune.co.nz/page/ohakune-useful-information/12/ [Accessed: 4-Mar.-2020].
[113] Environmental Protection Authority. Summary and Analysis – Carrots and Parsnips. No. APP201045, 2012. Available: https://www.epa.govt.nz/assets/FileAPI/hsno-ar/APP201045/fb604d3064/APP201045-Summary-and-Analysis-Carrot-and-Parsnip.pdf [Accessed: 4-Mar.-2020].
[114] Hall P, Jack M. Bioenergy options for New Zealand – Analysis of large-scale bioenergy from forestry. No. 1124-2019-3124, Scion – Next Generation Biomaterials, 2009. Available: https://niwa.co.nz/sites/niwa.co.nz/files/imported/_data/assets/pdf_file/0007/95668/Large-scale-forestry-for-bioenergy.pdf [Accessed: 4-Mar.-2020].
[115] [dataset] Anderson B, Eyers D, Ford R, Ocampo DG, Peniamina R, Stephenson J, et al. New Zealand GREEN Grid Household Electricity Demand Study 2014–2018. Colchester, Essex: UK Data Service. https://doi.org/10.5255/UKDA-SN-853334.
[116] Anderson J. Pulling the plug on network congestion. [B.A. dissertation]. Dunedin, New Zealand: Department of Economics, University of Otago; 2009.
[117] Tayan O, Alginahi YM, Kabir MN, Al Binali AM. Analysis of a transportation system with correlated network intersections: a case study for a central urban city with high seasonal fluctuation trends. IEEE Access 2017;5:7619–35. https://doi.org/10.1109/ACCESS.2017.2695159.
[118] The Electricity Market Information: The New Zealand Electricity Authority's wholesale database. [Online]. Available: https://www.emi.ea.govt.nz/Wholesale/Reports/ [Retrieved: 12-Feb.-2020].
[119] Concept Economics Pty Ltd. Investigation of the value of unserved energy – Stage 1. No. ABN 73 129 990 530, Prepared for Electricity Commission; 2008. Available: https://www.researchgate.net/profile/Deb_Chattopadhyay/publication/322255908_Investigation_of_the_Value_of_Unserved_Energy/links/5a4e8ff5458515e71b085a3f/Investigation-of-the-Value-of-Unserved-Energy.pdf [Accessed: 19-Dec.-2020].
[120] Xi X, Sioshansi R. Using price-based signals to control plug-in electric vehicle fleet charging. IEEE Trans Smart Grid 2014;5(3):1451–64. https://doi.org/10.1109/TSG.2014.2301931.
[121] Nwulu NI, Xia X. Multi-objective dynamic economic emission dispatch of electric power generation integrated with game theory based demand response programs. Energy Convers Manag 2015;89:963–74. https://doi.org/10.1016/j.enconman.2014.11.001.
[122] Nwulu NI, Xia X. Implementing a model predictive control strategy on the dynamic economic emission dispatch problem with game theory based demand response programs. Energy 2015;91:404–19. https://doi.org/10.1016/j.energy.2015.08.042.
[123] Mani S, Sokhansanj S, Bi X, Turhollow A. Economics of producing fuel pellets from biomass. Appl Eng Agric 2006;22(3):421–6. https://doi.org/10.13031/2013.20447.
[124] Baghaee HR, Mirsalim M, Gharehpetian GB. Multi-objective optimal power management and sizing of a reliable wind/PV microgrid with hydrogen energy storage using MOPSO. J Intell Fuzzy Syst 2017;32(3):1753–73. https://doi.org/10.3233/JIFS-152372.
[125] Li B, Roche R, Paire D, Miraoui A. Sizing of a stand-alone microgrid considering electric power, cooling/heating, hydrogen loads and hydrogen storage degradation. Appl Energy 2017;205:1244–59. https://doi.org/10.1016/j.apenergy.2017.08.142.
[126] Mukherjee U, Maroufmashat A, Ranisau J, Barbouti M, Trainor A, Juthani N, et al. Techno-economic, environmental, and safety assessment of hydrogen powered community microgrids; case study in Canada. Int J Hydrogen Energy 2017;42(20):14333–49. https://doi.org/10.1016/j.ijhydene.2017.03.083.
[127] Kampman B, Bergsma G, Schepers B, Croezen H, Fritsche UR, Henneberg K, et al. BUBE: better use of biomass for energy - background report to the position paper of IEA RETD and IEA bioenergy. IEA RETD and IEA Bioenergy. No. 10.3844.56; 2010. Available: https://www.ieabioenergy.com/wp-content/uploads/2013/10/Better-Use-of-Biomass-for-Energy-Background-Report.pdf [Accessed: 4-Mar.-2020].
[128] Lai CS, Locatelli G, Pimm A, Wu X, Lai LL. A review on long-term electrical power system modeling with energy storage. J Cleaner Prod 2021;280:124298. https://doi.org/10.1016/j.jclepro.2020.124298.
[129] Hosseinalizadeh R, Shakouri GH, Amalnick MS, Taghipour P. Economic sizing of a hybrid (PV–WT–FC) renewable energy system (HRES) for stand-alone usages by an optimization-simulation model: Case study of Iran. Renew Sustain Energy Rev 2016;54:139–50. https://doi.org/10.1016/j.rser.2015.09.046.
[130] Shang C, Srinivasan D, Reindl T. An improved particle swarm optimisation algorithm applied to battery sizing for stand-alone hybrid power systems. Int J Electr Power Energy Syst 2016;74:104–17. https://doi.org/10.1016/j.ijepes.2015.07.009.
[131] Fu R, Feldman DJ, Margolis RM. US solar photovoltaic system cost benchmark: Q1 2018. No. NREL/TP-6A20-72399. Golden, CO, USA: National Renewable Energy Lab (NREL); 2018.
[132] Li C. Techno-economic study of off-grid hybrid photovoltaic/battery and photovoltaic/battery/fuel cell power systems in Kunming, China. Energy Sources Part A Recover Util Environ Eff 2019;41(13):1588–604. https://doi.org/10.1080/15567036.2018.1549134.
[133] Rezk H, Sayed ET, Al-Dhaifallah M, Obaid M, El-Sayed AHM, Abdelkareem MA, et al. Fuel cell as an effective energy storage in reverse osmosis desalination plant powered by photovoltaic system. Energy 2019;175:423–33. https://doi.org/10.1016/j.energy.2019.02.167.